HHS Public Access

Author manuscript

SIAM J Numer Anal. Author manuscript; available in PMC 2017 October 03.

Published in final edited form as:

SIAM J Numer Anal. 2017 ; 55(2): 570–597. doi:10.1137/15M1040244.

ACCURATE SOLUTION AND GRADIENT COMPUTATION FOR ELLIPTIC INTERFACE PROBLEMS WITH VARIABLE COEFFICIENTS

ZHILIN LI[*], **HAIFENG JI**[†], and **XIAOHONG CHEN**[‡]

[*]Center for Research in Scientific Computation and Department of Mathematics, North Carolina State University, Raleigh, NC 27695, USA

[†]School of Science, Nanjing University of Posts and Telecommunications, Nanjing 210023, Jiangsu, China & Jiangsu Key Laboratory for NSLSCS, Nanjing 210023, Jiangsu, China

[‡]Department of Mathematics, North Carolina State University, Raleigh, NC 27695, USA

Abstract

A new augmented method is proposed for elliptic interface problems with a piecewise variable coefficient that has a finite jump across a smooth interface. The main motivation is not only to get a second order accurate solution but also a second order accurate gradient *from each side of the interface*. The key of the new method is to introduce the jump in the normal derivative of the solution as an augmented variable and re-write the interface problem as a new PDE that consists of a leading Laplacian operator plus lower order derivative terms near the interface. In this way, the leading second order derivatives jump relations are independent of the jump in the coefficient that appears only in the lower order terms after the scaling. An upwind type discretization is used for the finite difference discretization at the irregular grid points near or on the interface so that the resulting coefficient matrix is an M-matrix. A multi-grid solver is used to solve the linear system of equations and the GMRES iterative method is used to solve the augmented variable. Second order convergence for the solution and the gradient from each side of the interface has also been proved in this paper. Numerical examples for general elliptic interface problems have confirmed the theoretical analysis and efficiency of the new method.

Keywords

Elliptic interface problem; accurate gradient computation; variable coefficient with discontinuity; interface; M-matrix; convergence proof; discrete Green function

1. Introduction

In this paper, we develop an efficient numerical method to solve an elliptic interface problem

---

AMS subject classifications. 65M06, 65M85, 76M20.

$$\nabla \cdot (\beta(\mathbf{x})\nabla u(\mathbf{x}))=f(\mathbf{x}), \quad \mathbf{x} \in \Omega\backslash\Gamma, \quad \Omega=\Omega^+ \cup \Omega^-, \quad (1.1)$$

$$[u](\mathbf{X})=w(\mathbf{X}), \quad [\beta u_n](\mathbf{X})=v(\mathbf{X}), \quad \mathbf{X} \in \Gamma, \quad (1.2)$$

in one and two space dimensions, where for example, $[u] = [u]_\Gamma(\mathbf{X}) = u^+(\mathbf{X}) - u^-(\mathbf{X})$ is the difference of the limiting values of $u(\mathbf{X})$ from Ω^+ and Ω^- sides, respectively, $u_n=\mathbf{n} \cdot \nabla u=\frac{\partial u}{\partial n}$ is the normal derivative of solution $u(\mathbf{X})$, and $\mathbf{n}(\mathbf{X})$ is the unit normal direction at a point $\mathbf{X}$ on the interface pointing to Ω^+ side, see Fig. 1 for an illustration. The domain and the interface are used in Example 6.2 and Example 6.3 in Section 6. We use $\mathbf{x}$ to represent a point in the domain while $\mathbf{X}$ a point on the interface G. Since a finite difference discretization will be used, we assume that $f(\mathbf{x}) \in C(\Omega^\pm)$, $\beta(\mathbf{x}) \in C^1(\Omega^\pm)$, excluding Γ; and $\Gamma \in C^2$, $w \in C^2(\Gamma)$, $v \in C^1(\Gamma)$. All the parameters and $\frac{\partial \beta}{\partial x}$ and $\frac{\partial \beta}{\partial y}$ are assume to be bounded. For the regularity requirement of the problem, we also assume that $\beta(\mathbf{x}) \geq \beta_0 > 0$ and $f(\mathbf{x}) \in C^\nu(\Omega\backslash\Gamma)$, for a constant $\nu > 0$ so that $u(\mathbf{x}) \in C^{2+\nu}(\Omega^\pm)$, see [19, 8]. For the error analysis, piecewise higher regularity assumptions are needed for the solution, see Section 3 and Section 5.

Many free boundary and moving interface problems can be modelled by differential equations involving not only the solution to the governing equations, but also its gradient of the solution at the free boundary or moving interface from each side. Such examples include the Stefan problems and crystal growth modeling the interface between ice and water in which the velocity of the interface depends on the temperature of the heat equation and its gradient at the interface (called the Stefan condition), [12, 45]; the Hele-Shaw flow [30, 32]; the coupling between a Darcy's system and Stokes or Navier-Stokes equations [36]; and open and traction problems [46, 50]. The most expensive part of simulations from our research on those problems is to solve one or several elliptic interface problems, for example, two generalized Helmholtz and one Poisson equations when we solve the 2D incompressible Navier-Stokes equations involving interface using the projection method [46]. The goal of this paper is to present an efficient new finite difference method based a uniform Cartesian mesh that not only provides accurate solution globally but also its *accurate gradient* from each side of the interface.

For the elliptic interface problem (1.1)–(1.2), the solution has low global regularity, lower than H^1 is $w \neq 0$. Thus, a direct finite difference or finite element method will not work, or work poorly. Nevertheless, it is reasonable to assume that the solution is piecewise smooth excluding the interface. For example, if the coefficient is a piecewise constant in each sub-domain, then the solution in each sub-domain is an analytic function in the interior, but has jump in the solution or/and the normal derivative due to the source or dipole distribution from the PDE limiting theory [33]. The gradient used in this paper is defined as the *liming gradient* from each side of the interface.

[1]Note that some of the proof is similar to the contents in Section 6.1.2 in [43].

Naturally, finite element methods can be and have been applied to solve the interface problem. It is well known that a second order accurate approximation to the solution of an interface problem with $w \equiv 0$ and $v \equiv 0$ can be generated by the Galerkin finite element method with the standard linear basis functions if the triangulation is aligned with the interface, that is, a body fitted mesh is used, see for example, [7, 9, 13, 66]. Some kind of posterior techniques or at least quadratic elements are needed in order to get second order accurate gradient from each side of the interface. The cost in the mesh generation coupled with unstructured linear solver is hardly competitive with the algorithm proposed in this paper in our opinion.

There are also quite a few finite element methods using Cartesian meshes. The immersed finite element (IFEM) was developed for 1D and 2D interface problems in [40] and [44], respectively. Since then, many IFEM methods and analysis have appeared in the literature, see for example, [14, 25], with applications in [48, 67]. The IFEM distinguishes from other FE methods in terms of degree of the freedom and structure of the coefficient matrix, for example, the extended finite element method (XFEM) in which enrichment functions are added near the interface [60]; unfitted finite element method based on the Nitsche's method in [23]. Other related work in this direction can be found in [10, 35, 20, 28] and others. Note that, the methods developed in [29, 31] using a Petrov-Galerkin finite elements discretization in which the non-conforming IFE space and the standard linear finite element space are used as the trial and test functional spaces, respectively. A partially penalty IFE method has been proposed in [49]. Another type of methods are based on discontinuous Galerkin [65, 53] or weak Galerkin[62] methods with some penalties. In those methods, some parameters are chosen to achieve the optimal convergence. In general, discontinuous or weak Galerkin methods are flexible because there are more choices of the degree of freedom, which in turn implies these types of methods may be computationally more expensive. Those methods are usually better suited for hyperbolic problems and conservation laws. Another interesting development is the spectral solution representation technique [4, 5, 6, 3, 34] which is also based on integral forms. In this technique, the interface problem is decomposed into two problems, one with zero interface data and the other with zero exterior boundary data which is solved by introducing an interface space $H_\Gamma(\Omega)$ and constructing an orthogonal basis of this space.

Finite difference methods have also played very important role in scientific computing and solving engineering problems. Advantages of finite difference methods based on Cartesian meshes include simplicity, easy to programming, and can utilize many existing fast solvers. Note that error estimates from finite element methods are based on integral forms which may not exactly predict the actual errors near the interface for being averaging out compared with that from finite difference methods that are based on the point-wise (L^∞) norm. Many new finite difference methods based Cartesian mesh have been developed for interface problems, see for example, the ghost fluid method [51], the matched boundary interface method [70], the kernel free boundary integral method [68], the virtual node method [27]. The Difference Potential method [16, 59] has been developed for 1D elliptic and parabolic problems in [1]. In [54], the difference potential method with second-order accuracy in the solution and in the gradient has been developed for elliptic interface problems with variable coefficients in [15]. The fourth-order extension of the method for the elliptic interface problems is developed in [2].

Most of numerical methods for interface problems based on structure meshes are between first and second order accurate for the solution but the accuracy for the gradient is usually one order lower. Note that the gradient recovering techniques for examples, [61, 69], hardly work for structured meshes because of the arbitraries of the interface and the underlying mesh. The mixed finite element approach and a few other methods that can find accurate solution and the gradient simultaneously in the entire domain are often lead to a saddle problem and are computational expensive which are not ideal choices if we are only interested in the accurate gradient near the interface or boundary. It is the purpose of this paper to develop a new method that has second order accurate solution globally and second order accurate gradient at the interface. Note that for Poisson equations with singular source along an interface, it has been proved in [8] that both the computed solution and gradient are second order accurate by a factor of log h in the infinity norm. In [39], an augmented immersed interface method (AIIM) is proposed to solve the elliptic interface problems with piecewise constant coefficient. Both of the solution and the gradient are shown to be second order accurate for all the examples, which will be proved in this paper. The method in [39] provided a clue for accurate gradient computation at the interfaces or boundaries. The method implicitly put the gradient near the interface as an unknown (augmented variable). While there are quite few accurate and consistent numerical methods for interface problems, the stability of those methods nevertheless often ignored. In [42], a maximum principle preserving scheme is proposed for variable discontinuous coefficients. A quadratic optimization is used in determine the finite difference coefficients at grid points near the interface so that the coefficient matrix is an M-matrix which is the key in the proof of the convergence of the method. This is another consideration for our method to keep the coefficient matrix to be an M-matrix.

In this paper, we propose a new approach that can provide second order solution globally and second order accurate gradient *only* along the interface for a variable coefficient that has a finite jump along the interface. The method has advantages of both of the methods in [39] and [42]. The idea is to introduce the jump in the normal derivative of the solution as an augmented variable. With the augmented variable, the immersed interface method is second order accurate both for the solution and first order derivatives [8, 58]. By a suitable transform of the PDE, the leading terms of the second order derivative jump relations needed for the IIM are independent of the coefficient. The lower order derivative terms at irregular grid points that are near or on the interface are discretized using an upwinding discretization within the centered five-point stencil. Thus the coefficient matrix of the finite difference equations is an M-matrix without using an optimization procedure in [42]. It has been shown that the finite difference solution is second order accurate if the augmented variable is also second order accurate. The augmented variable should be chosen so that the flux jump condition is satisfied. This leads to a second discretization involving the finite difference solution and the augmented variable. The GMRES iteration is utilized to solve the Schur complement for the augmented variable with a new preconditioning strategy. By using the estimates of the discrete Green function, we have shown that the augmented variable has second order accuracy, so is the finite difference solution subsequently.

The rest of the paper is organized as follows. In the next section, we explain the algorithm in one-dimension since it is easy to understand and explain followed by the convergence proof. In Section 4, we explain the algorithm in two dimensions followed again by the convergence analysis in Section 5. In Section 6, we present some two dimensional numerical examples. We conclude in the last section.

2. The one-dimensional algorithm

A model interface problem in one dimension has the following form

$$\begin{gathered}(\beta u_x)_x = f(x), \quad x \in (a,\alpha) \cup (\alpha, b), \\ u(a) = u_a, \quad u(b) = u_b, \quad [u]_\alpha = w, \quad [\beta u_x]_\alpha = v,\end{gathered} \qquad (2.1)$$

where $a < \alpha < b$ is an interface (a point). We assume that conditions for $\beta(x)$, $f(x)$ described in the introduction section hold with $\Omega^- = (a, \alpha)$ and $\Omega^+ = (\alpha, b)$. We will drop the subscripts α in the jump expressions such as $[u]_\alpha$ and $[\beta u_x]_\alpha$ and simply use $[u]$ and $[\beta u_x]$ if there is no confusion.

Let $x_i = a + ih$ be a uniform mesh with $h = (b - a)/N$ and $i = 0, 1, \cdots, N$. We define $q = [u_x]_\alpha$ as the augmented variable. Assume that $x_j \le \alpha < x_{j+1}$. We call x_j and x_{j+1} as *irregular* grid points while others are call *regular* grid points. The finite difference scheme at a regular grid point x_i, $i \ge j$ and $i \ge j + 1$ can be written as

$$\frac{\beta_{i-1/2}U_{i-1} - 2\overline{\beta}_i U_i + \beta_{i+1/2}U_{i+1}}{\overline{\beta}_i h^2} = \frac{f(x_i)}{\overline{\beta}_i}, \qquad (2.2)$$

where

$$\beta_{i-1/2} = \beta(x_i - h/2), \quad \beta_{i+1/2} = \beta(x_i + h/2), \quad \overline{\beta}_i = \frac{\beta_{i-1/2} + \beta_{i+1/2}}{2}. \qquad (2.3)$$

At the irregular grid points x_j and x_{j+1}, we use the following equivalent differential equation

$$u_{xx} + \frac{\beta_x u_x}{\beta} = \frac{f}{\beta}. \qquad (2.4)$$

This is one of the key ideas of the new augmented approach. In this way, we can get second jump conditions $[u_{xx}]$ in terms of lower order jump conditions and derivatives of the solution.

If we know the jump $[u_x] = q$ in addition to the original jump conditions $[u]$ and $[\beta u_x]$, then we know the following jump relations

$$[u]=w, \quad [u_x]=q, \\ [u_{xx}]=\left[\frac{f}{\beta}\right]-\frac{\beta_x^+ u_x^+}{\beta^+}+\frac{\beta_x^- u_x^-}{\beta^-}=\left[\frac{f}{\beta}\right]-\left[\frac{\beta_x}{\beta}\right]u_x^-=\frac{\beta_x^+}{\beta^+}q. \tag{2.5}$$

If $\beta_x(x_j)/\beta(x_j) \geq 0$, then the finite difference discretization at the irregular grid point x_j can be written as

$$\frac{U_{j-1}-2U_j+U_{j+1}}{h^2}+C^{FD}(U_{j-1},U_j,U_{j+1})+\frac{\beta_x(x_j)}{\beta(x_j)}\left(\frac{U_{j+1}-U_j}{h}+C\right)=\frac{f(x_j)}{\beta(x_j)}, \tag{2.6}$$

where C is a correction term, see [43]

$$C=-\frac{[u]}{h}-\frac{(x_{j+1}-\alpha)[u_x]}{h}=-\frac{w}{h}-\frac{(x_{j+1}-\alpha)\,q}{h}, \tag{2.7}$$

and $C^{FD}(U_{j-1}, U_j, U_{j+1})$ is part of the finite difference equation,

$$C^{FD}(U_{j-1},U_j,U_{j+1})=-\frac{[u]}{h^2}-\frac{(x_{j+1}-\alpha)[u_x]}{h^2}-\frac{(x_{j+1}-\alpha)^2[u_{xx}]}{2h^2} \\ =-\frac{w}{h^2}-\frac{(x_{j+1}-\alpha)\,q}{h^2}-\frac{(x_{j+1}-\alpha)^2[u_{xx}]}{2h^2}, \tag{2.8}$$

in which $[u_{xx}]$ is discretized by, see (2.5),

$$[u_{xx}]=\left[\frac{f}{\beta}\right]-\left[\frac{\beta_x}{\beta}\right]u_x^- -\frac{\beta_x^+}{\beta^+}q \\ \approx \begin{cases} \left[\frac{f}{\beta}\right]-\frac{\beta_x^+}{\beta^+}q-\left[\frac{\beta_x}{\beta}\right]\frac{U_j-U_{j-1}}{h} & \text{if } \left[\frac{\beta_x}{\beta}\right]\leq 0, \\ \left[\frac{f}{\beta}\right]-\frac{\beta_x^+}{\beta^+}q-\left[\frac{\beta_x}{\beta}\right]\left(\frac{U_{j+1}-U_j}{h}+C\right) & \text{otherwise.} \end{cases}$$

The case when $\beta_x(x_j)/\beta(x_j) < 0$ can be treated in the similar way. We omit the details here. We can derive a similar finite difference scheme at the irregular grid point x_{j+1}. The finite difference scheme has the following properties.

- It is consistent. The local truncation errors at regular grid points are of $O(h^2)$, and $O(h)$ at irregular grids points x_j and x_{j+1}.
- The finite difference scheme can be written as

$$A_h \mathbf{U} + BQ = \mathbf{F}_1 \quad (2.9)$$

where the coefficient matrix A_h is an M-matrix, irreducible, tri-diagonal, and diagonally dominant, **U** is the column vector formed by the finite difference solution, and B is a column vector with at most two nonzero entries at j-th and $(j + 1)$-th locations, Q is the approximate value of $q = [u_x]$. Note that A_h is invertible and the two component of F_j and F_{j+1} have been modified.

2.1. Discretization of the flux jump condition

Next we discuss the interpolation scheme to approximate the interface condition $[\beta u_x] = v$. First we re-write the jump condition as follows

$$\begin{aligned}[\beta u_x] &= \beta^+ u_x^+ - \beta^- u_x^- = \beta^+ (u_x^- + q) - \beta^- u_x^- \\ &\Rightarrow \frac{\beta^+ - \beta^-}{\beta^+} u_x^- + q = \frac{v}{\beta^+}.\end{aligned} \quad (2.10)$$

This can be discretized as

$$\frac{\beta^+ - \beta^-}{\beta^+} \left(\gamma_1 U_{j-1} + \gamma_2 U_j + \gamma_3 U_{j+1} + C_3\right) + q = \frac{v}{\beta^+}, \quad (2.11)$$

where γ_1, γ_2, γ_3, and the correction term C_3 are determined again using the idea of the IIM so that the interpolation scheme is a second order approximation of (2.10), that is,

$$\frac{\beta^+ - \beta^-}{\beta^+} \left(\gamma_1 u(x_{j-1}) + \gamma_2 u(x_j) + \gamma_3 u(x_{j+1}) + C_3\right) + [u_x] - \frac{v}{\beta^+} = O(h^2).$$

In the matrix-vector form, the above equation can be written as

$$S\mathbf{U} + GQ = F_2 \quad (2.12)$$

where S is a row vector whose sum is zero.

We define the residual of the flux jump condition given an approximation Q as

$$R(Q) = S\mathbf{U} + GQ - F_2, \quad (2.13)$$

which is the discrete form of $r(q) = [\beta u_x] - v$. If we put the two equations (2.9) and (2.12) together, we get

$$\begin{bmatrix} A_h & B \\ S & G \end{bmatrix} \begin{bmatrix} \mathbf{U} \\ Q \end{bmatrix} = \begin{bmatrix} \mathbf{F}_1 \\ F_2 \end{bmatrix}. \quad (2.14)$$

Eliminating **U** in equation (2.14) gives the Schur complement equation for Q

$$(G - SA_h^{-1}B)Q = F_2 - SA_h^{-1}\mathbf{F}_1. \quad (2.15)$$

The equation (2.15) can be solved if the Schur complement is nonsingular. Once Q is computed, one can substitute it in equation (2.9) to solve for **U**. The cost of computation in this process is to solve linear systems with the form $A_h x = b$ three times, $A_h^{-1}\mathbf{F}_1$, $A_h^{-1}BQ$, and finally (2.9). Since matrix A_h is tridiagonal and row diagonally dominant, the Thomas algorithm is guaranteed to be stable and the solution can be obtained in $O(N)$ operations.

3. Convergence analysis of the 1D algorithm

In this section, we show second order convergence of the solution globally and its first order derivative at the interface, as well as the augmented variable of the proposed new method. The proof is simpler than that of the two dimensional case but serves the purpose of understanding and the tools used in the proof.

We use the following notations. We denote the errors as $\mathbf{E}^u = \mathbf{U} - \mathbf{u}$ with $\mathbf{E}_i^u = U_i - u(x_i)$ for the solution and $E^q = Q - q$ for the augmented variable, respectively, where $u(x_i)$ is the true solution at x_i. We use C to represent a generic error constant. We start with the analysis by assuming that the coefficient $\beta(x)$ is a piecewise constant, the domain is (0, 1), and a Dirichlet boundary condition at the two end points for simplicity.

Theorem 3.1: *Assume that $\beta(x)$ is a piecewise constant and $u(x)$ is in piecewise C^4 excluding the interface α. If Q is a second order accurate approximation to q, i.e. $|E^q| \le Ch^2$, then we also have $\|\mathbf{E}^u\|_\infty \le Ch^2$.*

Proof: Let $\mathbf{T}^u$ be the local truncation error of system (2.9), that is,

$$A_h\mathbf{u} + Bq = \mathbf{F}_1 + \mathbf{T}^u, \quad (3.1)$$

where **u** is the vector formed by the true solution at the grid points x_i, q is the jump of the derivative of the solution $[u_x]$ across the interface α. Subtracting equation (3.1) from (2.9) yields

$$A_h \mathbf{E}^u = \tilde{\mathbf{F}}^u, \quad (3.2)$$

where $\tilde{\mathbf{F}}^u = -\mathbf{T}^u - BE^q$. Notice that $|\mathbf{T}_i^u| \le Ch^2$ and $B_i = 0$ at regular grid points while $|\mathbf{T}_j^u| \le Ch$ and $|\mathbf{T}_{j+1}^u| \le Ch$, and $B_j \sim O(\frac{1}{h}),\ B_{j+1} \sim O(\frac{1}{h})$. Since $|E^q| \le Ch^2$, we have $\tilde{F}_i^u \approx O(h^2)$ at regular points while $\tilde{F}_j^u \sim O(h),\ \tilde{F}_{j+1}^u \sim O(h)$. Also when β is piecewise constant, the matrix A_h can be simplified as

$$A_h = \frac{1}{h^2} \begin{bmatrix} -2 & 1 & & \\ 1 & -2 & 1 & \\ \cdots & \cdots & \cdots & \cdots \\ & & 1 & -2 \end{bmatrix}.$$

From [37], we have

$$(A_h)_{ij}^{-1} = hG(x_i; x_j) = \begin{cases} h(x_j - 1)x_i, & i = 1, 2, \ldots, j, \\ h(x_i - 1)x_j, & i = j, j+1, \ldots, N-1, \end{cases} \quad (3.3)$$

where

$$G(x; \overline{x}) = \begin{cases} (\overline{x} - 1)x, & x \le \overline{x}, \\ (x - 1)\overline{x}, & x \ge \overline{x}, \end{cases}$$

is the Green's function that is the solution of the following

$$\begin{gathered} \Delta_x G(x; \overline{x}) = \delta(x - \overline{x}), \quad 0 < x < 1, \quad 0 < \overline{x} < 1, \\ G(0; \overline{x}) = 0, \quad G(1; \overline{x}) = 0. \end{gathered}$$

The global error of u then can be represented as

$$E_i^u = h \sum_{j=1}^{N-1} \tilde{F}_j^u G(x_i; x_j). \quad (3.4)$$

Since $0 \le G(x_i; x_j) \le 1$, we have the inequality

$$|E_i^u| \le \left|h\sum_{j=1}^{N-1}\tilde{F}_j^u\right| \le h\left(|\tilde{F}_j^u|+|\tilde{F}_{j+1}^u|+\sum_{k=1}^{j-1}|\tilde{F}_k|+\sum_{k=j+2}^{N-1}|\tilde{F}_k|\right)\sim h\left(O(h)+(N-2)O(h^2)\right)\sim O(h^2),$$

since $N \sim 1/h$. This shows that $\|E^u\|_\infty \le Ch^2$, hence the proof is completed.

Next, we show that the Schur complement system is non-singular.

Theorem 3.2: *With the same assumptions as in Theorem 3.1 and $\beta^- \neq \beta^+$, then the coefficient matrix (a number for the 1D problem) of the Schur complement is non-singular.*

Proof: Note that from (2.9), that is, $A_h\mathbf{U}(Q) + BQ = \mathbf{F}_1$, we have $A_h^{-1}BQ=A_h^{-1}\mathbf{F}_1-\mathbf{U}(Q)$ and the Schur complement can be re-written as

$$\begin{aligned}(G-SA_h^{-1}B)\,Q&=GQ-SA_h^{-1}BQ=GQ-SA_h^{-1}\mathbf{F}_1+S\mathbf{U}(Q)\\&=(S\mathbf{U}(Q)+GQ)-(SA_h^{-1}\mathbf{F}_1+G\cdot 0)\\&=(S\mathbf{U}(Q)+GQ)-(S\mathbf{U}(0)+G\cdot 0)\\&=R(Q)-R(0).\end{aligned}$$

If $Q \neq 0$ and $\beta^- \neq \beta^+$, then $R(Q) \neq R(0)$. For the one-dimensional problem, we have $(G-SA_h^{-1}B)=(G-SA_h^{-1}B)\,1=R(1)-R(0)\neq 0^1$.

Now we are ready to show that the augmented variable Q is also second order accurate.

Theorem 3.3: *With the same assumptions as in Theorem 3.1 and $\beta^- \neq \beta^+$, then we have $|E^q| = |Q - q| \le Ch^2$.*

Proof: Similarly to the definition of the local truncation error $\mathbf{T}^u$, we define the local truncation T^q of q as

$$S\mathbf{u}+Gq=F_2+T^q, \quad (3.5)$$

where $\mathbf{u}$ and q are defined as before. From (2.14), we know that

$$\begin{bmatrix} A & B \\ S & G \end{bmatrix}\begin{bmatrix} \mathbf{E}^u \\ E^q \end{bmatrix}=\begin{bmatrix} -\mathbf{T}^u \\ -T^q \end{bmatrix}. \quad (3.6)$$

Eliminating $\mathbf{E}^u$, we get the Schur complement system for E^q

$$(G-SA^{-1}B)E^q=-T^q+SA^{-1}\mathbf{T}^u. \quad (3.7)$$

We already know that the $(G - SA^{-1}B)$ is non-singular and $\|T^q\|_\infty \le Ch^2$. The key is to show that $\|SA^{-1}\mathbf{T}^u\|_\infty \le Ch^2$.

Let $\mathbf{b} = A^{-1}\mathbf{T}^u$, from the definition of the Green function in (3.3), we can write

$$b_i=h\sum_{l=1}^{N-1}\mathbf{T}_j^u G(x_i;x_l). \quad (3.8)$$

At the first glance, it seems that $E^q \sim O(h)$ since the interpolation operator $\|S\|_\infty \sim 1/h$. Nevertheless, the following analysis shows that the terms of $O(1/h)$ are cancelled out to $O(1)$ and thus $E^q \sim O(h^2)$ is true. Let $\Delta_i = b_i - b_{i-1}$, $i = 2, \ldots, N - 1$. Then we have (note that both $SA^{-1}\mathbf{T}^u$ and $S\,\mathbf{b}$ are scalars for the 1D problem)

$$\begin{aligned} SA^{-1}\mathbf{T}^u=S\,\mathbf{b}&=S_{j-1}b_{j-1}+S_jb_j+S_{j+1}b_{j+1}\\ &=S_{j-1}(b_j-\Delta_j)+S_jb_j+S_{j+1}(b_j+\Delta_{j+1})\\ &=(S_{j-1}+S_j+S_{j+1})b_j-S_{j-1}\Delta_j+S_{j+1}\Delta_{j+1}\\ &=-S_{j-1}\Delta_j+S_{j+1}\Delta_{j+1}. \end{aligned}$$

Notice the term b_j is cancelled out. This is because the interpolation operator is for the first order derivative of $u(x)$, and the consistency condition requires that $S_{j-1} + S_j + S_{j+1} = 0$. Now what is left to prove is that $\Delta_j \sim \Delta_{j+1} \sim O(h^3)$, which leads to $E^q \sim h^2$ Since $S_{j-1} \sim S_{j+1} \sim O(1/h)$. The final step of the proof is explained below.

$$\begin{aligned} |\Delta_i|=|b_i-b_{i-1}|&=h\sum_{l=1}^{N-1}|\mathbf{T}_l^u|\cdot|G(x_i;x_l)-G(x_{i-1};x_l)|\\ \le h^2\sum_{l\neq j,j+1}^{N-1}|\mathbf{T}_l^u|+h^2(|T_j^u+|T_{j+1}^u|) &\quad \text{from the continuity of } G(x_i,x_l),\\ &\approx O(h^3). \end{aligned}$$

This completes the proof.

As the result of Theorem 3.1–Theorem 3.3, we conclude that the solution **U** is also second order approximation to **u**, which is summarized in the following theorem.

<u>Theorem 3.4:</u> *With the same assumptions as in Theorem 3.1 and $\beta^- \ne \beta^+$, and β is piecewise constant, then* $\|\mathbf{E}^u\|_\infty = \|\mathbf{U} - \mathbf{u}\|_\infty \le Ch^2$.

Proof: Since the Schur complement matrix is a constant independent of h and $|T^q| \le Ch^2$, and just proved $|SA^{-1}\mathbf{T}^u| \le Ch^2$, from (2.15), we have the conclusion.

Not only we get second order accurate solution and the augmented variable, but also second order accurate derivative u_x^- and u_x^+ if the derivative is computed using the scheme (2.10), that is,

$$u_x^- = \frac{\beta^+}{\beta^+ - \beta^-} \left(\frac{v}{\beta^+} - q \right), \quad (3.9)$$

assuming that $\beta^- \neq \beta^+$. Since the computed Q is second order accurate, we immediately have the following theorem.

Theorem 3.5: *Assume β is two different piecewise constants and U_x^- is computed using the above formula with q being replaced by Q, the computed augmented variable. Then*

$|U_x^- - u_x^-| \le Ch^2$, *where* $u_x^- = \lim_{x \to \alpha-} \frac{du}{dx}(x)$.

3.1. An example of the 1D Stefan problem

Our numerical experiments in one-dimension have confirmed our theoretical analysis that both of the solution $\mathbf{U} \approx u(x)$ and the augmented variable $Q \approx [u_x]$ are second order accurate in the L^∞ norm. We show an example of 1D Stefan problem, see for example, [11, 18], in which the free boundary $\alpha(t)$ is moving. The governing equations are

$$\begin{array}{lll} \frac{\partial u}{\partial t} = \frac{\partial^2 u}{\partial x^2}, & \text{for} \quad 0 < x < \alpha(t), & t > 0, \\ u(x,t) = 0, & \text{for} \quad x \ge \alpha(t), & t > 0, \end{array}$$

where $\alpha(t)$ is subject to the Stefan condition

$$\frac{d\alpha}{dt}(t) = -\frac{\partial u}{\partial x}(\alpha(t), t), \qquad \alpha(0) = 0.$$

The boundary and initial conditions are

$$\frac{\partial u}{\partial x}(0,t) = f(t), \qquad u(\alpha(t), t) = 0, \qquad u(x,0) = 0.$$

The model is from [55]. We can find an analytic solution listed below,

$$u(x,t) = 1 - \frac{\operatorname{erf}(x/(2\sqrt{t}))}{\operatorname{erf}(\omega)}, \qquad \alpha(t) = 2\omega\sqrt{t},$$

where erf is the error function and ω is the solution of the transcendental equation $\sqrt{\pi}\omega \cdot \mathrm{erf}(\omega)e^{\omega^2}=1$. The function $f(t, \alpha(t))$ is determined from the analytic solution.

We use a second order time splitting technique to solve the problem, that is, solve the differential equation with $\alpha(t)$ fixed, then update the new location of $\alpha(t)$. The augmented equation now is the boundary condition at $\alpha(t)$. In Table 1, we show a grid refinement analysis of the errors in the solution at all grid points, and the free boundary $\alpha(t)$, and the first order derivative $u_x^-(\alpha(t))$, at the final time $t = 3$. We use the lower case for the analytic solution, and the upper case as the computed solutions. We observe that all of them have average second order convergence.

4. The algorithm for two dimensional problems

In this section, we present the algorithm for two dimensional problems. The key is the modification of the finite difference scheme at irregular grid points. We first discuss the interface relations using an equivalent representation of the interface problem.

4.1. The jump relations in the local coordinates

As explained in the introduction section, we re-write the elliptic interface problem near the interface as

$$\Delta u+\frac{\beta_x}{\beta}u_x+\frac{\beta_y}{\beta}u_y=\frac{f}{\beta}, \qquad (4.1)$$

$$[u]_\Gamma=w, \quad [u_n]_\Gamma=q, \qquad (4.2)$$

where $q(\mathbf{X})$ is the augmented variable only defined along the interface G which should be chosen such that the flux jump condition

$$[\beta u_n]_\Gamma(\mathbf{X})=v(\mathbf{X})$$

is satisfied. In this way, the Laplacian term Δu has been separated from $\beta(x, y)$ which makes the discretization easier with our proposed augmented method. This is one of the key ideas of the new method.

From the description of Section 3.1 in [38, 43], we restate some theoretical results on the reformulated elliptic interface problem (4.1)–(4.2). Assume that the interface in the parametric form is

$$\Gamma=\left\{(X(s),Y(s)),\quad X(s)\in C^2,\,Y(s)\in C^2\right\}, \quad (4.3)$$

where s is a parameter, for example, the arc-length. At a point of the interface (X, Y), the local coordinate system in the normal and tangential directions is defined as (see Figure 2 for an illustration),

$$\begin{cases} \xi=(x-X)\cos\theta+(y-Y)\sin\theta \\ \eta=-(x-X)\sin\theta+(y-Y)\cos\theta, \end{cases} \quad (4.4)$$

where θ is the angle between the x-axis and the normal direction, pointing to the Ω^+ sub-domain. Under such new coordinates system, the interface can be parameterized as

$$\xi=\chi(\eta) \quad \text{with} \quad \chi(0)=0, \quad \chi^{'}(0)=0. \quad (4.5)$$

The curvature of the interface at (X, Y) is $\chi''(0)$.

If we know the jump in the solution $[u] = w$ and the normal derivative $[u_n] = q$ (not the original flux jump condition $[\beta u_n] = v$), then we can have the following jump relations at a point (X, Y) on the interface which is necessary to derive the accurate finite difference method.

Theorem 4.1: *For the elliptic interface problem* (4.1)–(4.2), *given* $[u] = w$ *and* $[u_n] = q$, *then at the interface, the following jump relations hold*

$$\begin{gathered} [u]=w, \quad [u_\eta]=w^{'}, \quad [u_\xi]=q, \\ [u_{\eta\eta}]=-q\chi^{''}+w^{''}, \quad [u_{\xi\eta}]=w^{'}\chi^{''}+q^{'}, \\ [u_{\xi\xi}]=q\left(\chi^{''}-\frac{\beta_\xi^+}{\beta^+}\right)-w^{''}-\left[\frac{\beta_\xi}{\beta}\right]u_\xi^- -\left[\frac{\beta_\eta}{\beta}\right]u_\eta^- -\frac{\beta_\eta^+}{\beta^+}w^{'}+\left[\frac{f}{\beta}\right] \end{gathered} \quad (4.6)$$

where w', g' and w'' are the first and second order surface derivatives of w and g on the interface, which are all evaluated at $(\xi,\eta) = (0, 0)$. Here we skip the derivation which is similar to those derived in equation (3.5) in Section 3.1 in [43] assuming that $[u] = w$ and $[\beta u_n] = v$ are given. Note also that we can express the jump conditions in terms of u^+, u_η^+, and u_ξ^+.

Once we have the jump relations in the local coordinates, we can get back the jump relations in the x- and y- directions according to (9.47) in [43]

$$[u_x]=[u_\xi]\cos\theta-[u_\eta]\sin\theta, \quad [u_y]=[u_\xi]\sin\theta+[u_\eta]\cos\theta,$$
$$[u_{xx}]=[u_{\xi\xi}]\cos^2\theta-2[u_{\xi\eta}]\cos\theta\sin\theta+[u_{\eta\eta}]\sin^2\theta,$$
$$[u_{yy}]=[u_{\xi\xi}]\sin^2\theta+2[u_{\xi\eta}]\cos\theta\sin\theta+[u_{\eta\eta}]\cos^2\theta. \qquad (4.7)$$

4.2. The finite difference scheme for the 2D problem

For simplification of discussion, we use a uniform a mesh

$$x_i=a+ih, \quad i=0,1,\cdots M; \quad y_j=c+jh, \quad j=0,1,\cdots,N, \qquad (4.8)$$

assuming Ω = (a, b) × (c, d). The interface G is represented by the zero level set of a Lipschitz continuous function $\varphi(x, y)$, that is

$$\Gamma=\{(x,y), \quad \varphi(x,y)=0, \quad (x,y)\in\Omega\}. \qquad (4.9)$$

In the neighborhood of the interface, we assume that $\varphi(x, y) \in C^2$. In implementation, the level set function is defined at the grid points as $\{\varphi_{ij}\}$ corresponding to $\varphi(x_i, y_j)$. At a grid point (x_i, y_j), we define

$$\varphi_{ij}^{max}=\max\{\varphi_{i-1,j},\varphi_{ij},\varphi_{i+1,j},\varphi_{i,j-1},\varphi_{i,j+1}\}, \qquad (4.10)$$

$$\varphi_{ij}^{min}=\min\{\varphi_{i-1,j},\varphi_{ij},\varphi_{i+1,j},\varphi_{i,j-1},\varphi_{i,j+1}\}. \qquad (4.11)$$

A grid point (x_i, y_j) is called *regular* if $\varphi_{ij}^{max}\varphi_{ij}^{min}>0$, otherwise it is called *irregular*.

The set of orthogonal projections (X_k, Y_k), $k = 1, 2,\cdots, N_b$ of all irregular grid points on the interface from a particular side, say Ω^+ side, forms a discretization of the interface Γ. We refer the reader to Section 1.6.4 in [43] about how to find approximate orthogonal projections. Then the discrete augmented variable Q_k of the continuous one $q(s)$ is defined at those orthogonal projections. Given a discrete quantity along the interface, we can interpolate the quantity at the discrete points to get its value, the tangential derivative anywhere along the interface. For example, assume that (x_i, y_j) is an irregular grid point, and the interface cuts the grid line at (x_{ij}^*, y_j) corresponding to the orthogonal projection $\mathbf{X}_k = (X_k, Y_k)$. We need to get the values of Q and its tangential derivative at (x_{ij}^*, y_j). We first reconstruct the interface in the local coordinates as $\xi \approx C\eta^2 + D\eta^3$ with error $O(\eta^4)$. We refer the readers to Section 11.1.5 in [43] about how to find C and D. We then approximate $Q(\eta)$ as $Q(\eta) = Q_k + \omega_1\eta + \omega_2\eta^2$ locally with error $O(\eta^3)$ and $Q'(\eta) = \omega_1 + 2\omega_2\eta$ with error $O(h^2)$. The coefficient ω_1 and ω_2 are determined from Q values at the two closest orthogonal projections.

4.2.1. The finite difference scheme at a regular grid point—At a regular grid point (x_i, y_j), the finite difference scheme is the classic conservative one with the scaling

$$\frac{\beta_{i-1/2,j}U_{i-1,j}+\beta_{i+1/2,j}U_{i+1,j}+\beta_{i,j-1/2}U_{i,j-1}+\beta_{i,j+1/2}U_{i,j+1}-\overline{\beta}_{ij}U_{i,j}}{h^2\overline{\beta}_{ij}}=\frac{f_{ij}}{\overline{\beta}_{ij}} \quad (4.12)$$

where $f_{ij} = f(x_i, y_j)$, $\beta_{i-1/2,j} = \beta(x_i - h/2, y_j)$ and so on, and

$$\overline{\beta}_{ij}=\beta_{i-1/2,j}+\beta_{i+1/2,j}+\beta_{i,j-1/2}+\beta_{i,j+1/2}. \quad (4.13)$$

4.2.2. The finite difference scheme at an irregular grid point—We assume that we know the jump conditions $[u] = w$ and $[u_n] = q$, not the original flux jump condition $[\beta u_n] = v$. This makes it easier to derive accurate and stable finite difference scheme. At an irregular grid point, we discretize the re-written equation (4.1) using a dimension by dimension approach, and an upwinding discretization for the first order derivative terms.

Let (x_i, y_j) be an irregular grid point. If the interface does not cut through the interval (x_{i-1}, x_{i+1}) along the line $y = y_j$, that is, (x_i, y_j) is regular in the x-direction, then the finite difference approximation for $(\beta u_x)_x$ before the scaling is

$$(\beta u_x)_x \approx \frac{\beta_{i-1/2,j}U_{i-1,j}+\beta_{i+1/2,j}U_{i+1,j}-(\beta_{i-1/2,j}+\beta_{i+1/2,j})U_{i,j}}{h^2}. \quad (4.14)$$

The final finite difference equation will be scaled in the similar way as those at regular grid points.

Now assume the interface cuts the grid line $y(x) = y_j$ in the interval (x_{i-1}, x_{i+1}), say at (x_{ij}^*, y_j), with $x_{ij}^*=x_i+\alpha_{ij}^x h,\ 0 \le |\alpha_{ij}^x|<1$. Without lost of generality, we assume that $(x_i, y_j) \in \Omega^-$. We discretize the reformulated equation (4.1), that is,

$$u_{xx}^-+u_{yy}^-+\frac{\beta_x^- u_x^-}{\beta^-}+\frac{\beta_y^- u_y^-}{\beta^-}=\frac{f^-}{\beta^-}, \quad (4.15)$$

where f^-, β^-, $\cdots$, are the limiting values at (x_{ij}^*, y_j) from Ω^- side. We use an upwinding scheme for the first order term $\beta_x^- u_x^-/\beta^-$, that is,

$$\frac{\beta_x^- u_x^-}{\beta^-} \approx \begin{cases} \frac{\beta_x^-}{\beta^-}\left(\frac{U_{i,j}-U_{i-1,j}}{h}+\frac{\tilde{C}_{ij}^x}{h}\right) & \text{if } \frac{\beta_x^-}{\beta^-} \le 0, \\ \frac{\beta_x^-}{\beta^-}\left(\frac{U_{i+1,j}-U_{i,j}}{h}+\frac{\tilde{C}_{ij}^x}{h}\right) & \text{otherwise,} \end{cases} \quad (4.16)$$

where for example, $\tilde{C}_{ij}^x=0$ if $(x_{i-1}, y_j) \in \Omega^-$. Otherwise we have

$$\tilde{C}_{ij}^x=-\left([u]+[u_x]\,(1-|\alpha_{ij}^x|)\,h\right), \quad \text{where} \quad \alpha_{ij}^x=\frac{x_{ij}^*-x_i}{h}, \quad (4.17)$$

see Lemma 10.6 in [43] for the formulas of the correction, where the jumps again are defined at (x_{ij}^*, y_j). Similarly, for the second order term u_{xx}, the finite difference approximation for u_{xx} can be written as

$$u_{xx}^-(x_i, y_j) \approx \frac{U_{i-1,j}-2U_{i,j}+U_{i+1,j}-C_{ij}^x}{h^2}, \quad (4.18)$$

where the correction term C_{ij}^x is

$$C_{ij}^x=[u]+[u_x]\,(1-|\alpha_{ij}^x|)\,h+[u_{xx}]\frac{(1-|\alpha_{ij}^x|)^2h^2}{2}. \quad (4.19)$$

4.2.3. Approximating $[u_{xx}]$ and $[u_{yy}]$—Given $[u] = w$ and $[u_n] = q$ along the interface, from (4.7) and (4.6) we have the following

$$\begin{aligned} &[u_x]=\cos\theta\,[u_\xi]-\sin\theta\,[u_\eta]=q\cos\theta-w'\sin\theta, \\ &[u_y]=\sin\theta\,[u_\xi]+\cos\theta\,[u_\eta]=q\sin\theta+w'\cos\theta, \\ &[u_{xx}]=\cos^2\theta\,[u_{\xi\xi}]-2\sin\theta\cos\theta\,[u_{\xi\eta}]+\sin^2\theta\,[u_{\eta\eta}] \\ &=-2\sin\theta\cos\theta\,(w'\chi''+q')+\sin^2\theta\,(-q\chi''+w'')+\cos^2\theta\left\{q\left(\chi''-\frac{\beta_\xi^+}{\beta^+}\right)-w''-\frac{\beta_\eta^+}{\beta^+}w'+\left[\frac{f}{\beta}\right]-\left[\frac{\beta_\xi}{\beta}\right](\cos\theta\,u_x^-+\sin\theta\,u_y^-)-\left[\frac{\beta_\eta}{\beta}\right](-\sin\theta\,u\right. \end{aligned}$$

$$\begin{aligned} &[u_{yy}]=\sin^2\theta\,[u_{\xi\xi}]+2\sin\theta\cos\theta\,[u_{\xi\eta}]+\cos^2\theta\,[u_{\eta\eta}] \\ &=2\sin\theta\cos\theta\,(w'\chi''+q')+\cos^2\theta\left(-q\chi''+w''\right)+\sin^2\theta\left\{q\left(\chi''-\frac{\beta_\xi^+}{\beta^+}\right)-w''-\frac{\beta_\eta^+}{\beta^+}w'+\left[\frac{f}{\beta}\right]-\left[\frac{\beta_\xi}{\beta}\right](\cos\theta\,u_x^-+\sin\theta\,u_y^-)-\left[\frac{\beta_\eta}{\beta}\right](-\sin\theta u\right. \end{aligned}$$

where w' and q' are the first order, and w'' is the second order, derivatives along the interface, respectively. In the derivation above, we have used the following formulas

$$u_\xi = u_x \cos\theta + u_y \sin\theta, \quad u_y = -u_x \sin\theta + u_y \cos\theta. \quad (4.20)$$

Most of terms in $[u_{xx}]$ and $[u_{yy}]$ are computable except terms of u^-, u_x^- and u_y^-. Note that these functions are defined on the interface. Using Taylor expansion, we have $u^-(X, Y) = u^-(x_i, y_j) + O(h)$, $u_x^-(X,Y) = u_x^-(x_i, y_j) + O(h)$ and $u_y^-(X,Y) = u_y^-(x_i, y_j) + O(h)$. We simply replace u^- with U_{ij} and treat u_x^- and u_y^- using the upwinding scheme to increase the diagonal dominance of the resulting linear system of finite difference equations. For example, for the terms containing u_x^- in $[u_{xx}]$ we use

$$\left(\left[\frac{\beta_\eta}{\beta} \right] \sin\theta - \left[\frac{\beta_\xi}{\beta} \right] \cos\theta \right) \cos^2\theta \, u_x^- = \begin{cases} A_{tmp} \left(\frac{U_{i+1,j} - U_{i,j}}{h} + \frac{\tilde{C}_{ij}^x}{h} \right) & \text{if } A_{tmp} \geq 0, \\ A_{tmp} \left(\frac{U_{i,j} - U_{i-1,j}}{h} + \frac{\overline{C}_{ij}^x}{h} \right) & \text{otherwise,} \end{cases}$$
$$\text{where} \quad A_{tmp} = \left(\left[\frac{\beta_\eta}{\beta} \right] \sin\theta - \left[\frac{\beta_\xi}{\beta} \right] \cos\theta \right) \cos^2\theta,$$

and once again, for example, $\tilde{C}_{ij}^x = 0$ if $(x_{i-1}, y_j) \in \Omega^-$. Otherwise

$$\tilde{C}_{ij}^x = -\left([u] + [u_x] (1 - |\alpha_{ij}^x|) \, h \right). \quad (4.21)$$

The linear system of finite difference equations can be written as

$$A_h \mathbf{U} + B \mathbf{Q} = \mathbf{F}_1, \quad (4.22)$$

where **U** is the vector formed by the finite difference approximation $\{U_{ij}\}$ to the solution $\{u(x_i, y_j)\}$, **Q** is the vector formed by the discrete augmented variable $\{Q_k\}$ to the augmented variable $\{[\frac{\partial u}{\partial n}(X_k, Y_k)]\}$, F_1 is the modified right hand side, B is a sparse matrix corresponding to the correction terms for the $[u_n]$ term.

Remark 4.2

- *The finite difference stencil is still standard five-point centered. This is different from the maximum principal preserving scheme* [42] *in which the finite difference stencil is a nine-point one.*
- *A_h is an M-matrix and irreducible, thus it is invertible. No optimization is needed compared to that in* [42] *because we assume that $[u_n]$ is given instead of $[\beta u_n]$, which makes easier to discretize the interface problem. The trade-off is that we also need to solve the augmented variable.*

4.3. Discretizing the flux jump condition

At every approximate orthogonal projections of all irregular grid points on the interface, we use the same least squares interpolation described in Section 4 in [39] to interpolate the flux jump condition $[\beta u_n] = v$.

At one orthogonal projection $\mathbf{X}_k = (X_k, Y_k)$ corresponding to an irregular grid point (x_i, y_j), the second order accurate least squares interpolation scheme approximating $[\beta u_n] = v$ can be written as

$$\sum_{|\mathbf{x}_{ij}-\mathbf{X}_k| \le \delta_h} \gamma_{ij} U_{ij} + L_k\left(\beta(\mathbf{x}), \mathbf{W}, \mathbf{Q}, \mathbf{V}\right) = 0 \qquad (4.23)$$

where δ_h is a parameter of $2h \sim 3h$, L_k stands for a linear relation of its augmenters, the discrete form of $w(\mathbf{X})$, $q(\mathbf{X})$, and $v(\mathbf{X})$. The consistency condition requires that

$$\sum_{|\mathbf{x}_{ij}-\mathbf{X}_k| \le \delta_h} \gamma_{ij} = 0. \qquad (4.24)$$

Note that the interpolation coefficients should depend on the index k as well, we omit it for simplicity of notations.

In the matrix vector form, the interpolation at all projections of irregular grid points from one particular side can be written as

$$S\mathbf{U} + G\mathbf{Q} = \mathbf{F}_2, \qquad (4.25)$$

for some sparse matrices S and G. If we put (4.22) and (4.25) together we get

$$\begin{bmatrix} A_h & B \\ S & G \end{bmatrix} \begin{bmatrix} \mathbf{U} \\ \mathbf{Q} \end{bmatrix} = \begin{bmatrix} \mathbf{F}_1 \\ \mathbf{F}_2 \end{bmatrix}. \qquad (4.26)$$

Eliminating U in equation (4.26) gives the Schur complement equation for $\mathbf{Q}$

$$(G - SA_h^{-1}B)\mathbf{Q} = \mathbf{F}_2 - SA_h^{-1}\mathbf{F}_1, \quad \text{or} \quad A_h^{schur}\mathbf{Q} = \mathbf{F}^{schur}. \qquad (4.27)$$

We use the GMRES iterative method to solve the Schur complement system and do not explicitly form the matrices A_h, B, S, G, and A_h^{schur}. The matrix and vector multiplication $A_h^{schur}\mathbf{Q}$ needed for the GMRES iteration involves two consecutive steps: the first step is to solve the interface problem (4.22) given **Q**; the second step is to find the residual of the flux jump condition, that is, $R(\mathbf{Q}) = [\beta(\mathbf{X})\mathbf{U}_n(\mathbf{Q})] - \mathbf{V}$. We refer the readers to Section 5.1 in [39] for the details.

4.4. Computing the gradient on the interface

At one orthogonal projection $\mathbf{X}_k$ corresponding to an irregular grid point (x_i, y_j), we use a similar (two-sided SVD) interpolation to approximate the normal derivative at $\mathbf{X}_k$ from Ω^- side

$$u_n^-(\mathbf{X}_k)=\sum_{|\mathbf{x}_{ij}-\mathbf{X}_k|\leq\delta_h}\widetilde{\gamma_{ij}}\,U_{ij}+\widetilde{L_k}\,(\beta(\mathbf{x}),\mathbf{W},\mathbf{Q},\mathbf{V}) \qquad (4.28)$$

to get one of $u_n^-(\mathbf{X}_k)$ or $u_n^+(\mathbf{X}_k)$, then use $q(\mathbf{X}_k)$ to get the other, say $u_n^+(\mathbf{X}_k)=q(\mathbf{X}_k)+u_n^-(\mathbf{X}_k)$. The linear system of equations has the same coefficient matrix as that in (4.23) for γ_{ij}'s, so there is almost no additional cost. The term $\widetilde{L_k}\,(\beta(\mathbf{x}),\mathbf{W},\mathbf{Q},\mathbf{V})$ is again a correction term due to the jumps in the involved quantities.

If needed, at a grid point, the partial derivatives u_x and u_y can be calculated using the standard 3-point central finite difference formula with (at an irregular grid point) or without (at a regular grid point) a correction term. Beadle and Layton [8] have shown that the computed derivatives using IIM are second order accurate in the L^∞ norm at all grid points.

4.5. A new preconditioning strategy

The number of GMRES iteration grows linearly with the mesh size N if there is no preconditioning technique employed. The preconditioning technique proposed in [39] works well for a piecewise constant coefficient but not for a variable coefficient. The idea of new preconditioning technique is more like a diagonal preconditioning technique for the Schur complement. At an orthogonal projection $\mathbf{X}_k = (X_k, Y_k)$ where the augmented variable is defined, we use the re-scaled residual of the flux jump condition

$$R^{rescaled}(\mathbf{X}_k)=\frac{\beta^+(\mathbf{X}_k)U_n^+(\mathbf{X}_k)-\beta^-(\mathbf{X}_k)U_n^-(\mathbf{X}_k)-v(\mathbf{X}_k)}{\overline{\beta}(\mathbf{X}_k)}, \qquad (4.29)$$

where $\bar{\beta}(\mathbf{X}_k) = (\beta^-(\mathbf{X}_k) + \beta^+(\mathbf{X}_k))/2$, to discretize the flux jump condition.

5. Convergence proof for the 2D Problems

In this section, we provide a convergence proof for two dimensional problems. For simplicity, we assume that a Dirichlet boundary condition is prescribed along the boundary $\partial\Omega$. We use **U** and **u** to represent the vectors of approximate and exact solution at grid points; $\mathbf{T}^u$ and $\mathbf{E}^u = \mathbf{U} - \mathbf{u}$ are the vectors of the local truncation errors and the global error. We have $\mathbf{E}^u|_{\partial\Omega_h} = \mathbf{0}$ for the values at grid points on the boundary. Similarly, we define $\mathbf{T}^q$ and $\mathbf{E}^q = \mathbf{Q}$

$-$ **q** as the vectors of the local truncation error and the global error for the augmented variable. According to the definition, we have

$$A_h\mathbf{U}+B\mathbf{Q}=\mathbf{F}_1, \quad A_h\mathbf{E}^u+B\mathbf{E}^q=\mathbf{T}^u, \quad (5.1)$$

$$S\mathbf{U}+G\mathbf{Q}=\mathbf{F}_2, \quad S\mathbf{E}^u+G\mathbf{E}^q=\mathbf{T}^q, \quad (5.2)$$

where the local truncation error vector $\mathbf{T}^u$ is defined as $\mathbf{T}^u = \mathbf{F}_1 - A_h\mathbf{u} - B\mathbf{q}$ and so on.

__Lemma 5.1:__ *Assume that* $u(\mathbf{x})$ *is in piecewise* $C^4(\Omega\backslash\Gamma)$ *excluding the interface* Γ*. If the augmented variable is a second order approximation to* $[\frac{\partial u}{\partial n}(\mathbf{X})]$*, that is,* $\|\mathbf{E}^q\|_\infty \le Ch^2$*, then the computed solution of the finite difference* equations (4.22) *is also second order accurate, that is,* $\|\mathbf{E}\|_\infty \le Ch^2$.

Proof: From the construction of the numerical scheme we know that a component of $B\mathbf{E}^q$ is zero at a regular grid point $\mathbf{x}_{ij}$ and bounded by Ch at an irregular grid point $\mathbf{x}_{ij}$ since $\|\mathbf{E}^q\|_\infty \le Ch^2$ as one of the conditions in the theorem. Note that A_h is an M-matrix and $A_h\mathbf{E}^u = -B\mathbf{E}^q + \mathbf{T}^u$ that is bounded by Ch^2 at regular grid points and Ch at irregular grid points. From Theorem 3.3 in [43] or the convergence analysis of IIM in [8], we conclude that the global error is bounded by Ch^2. Also from [57, 58], the partial derivatives using the IIM is also second order accurate.

The next part is to show that the computed augmented variable is also second order accurate by a factor of log h. In this case, we first assume that the coefficient is piecewise constant so that we can apply some theoretical results from [41].

__Theorem 5.2:__ *Assume that* $u(\mathbf{x})$ *is in piecewise* $C^4(\Omega\backslash\Gamma)$ *excluding the interface* Γ*, and the coefficient* $\beta(\mathbf{x})$ *is a piecewise constant* β^- *and* β^+*, then computed augmented variable is second order accurate by a fact of* $|\log h|$*, that is* $\|\mathbf{E}^q\|_\infty \le Ch^2|\log h|$.

Proof: From (5.1)–(5.2), we have

$$\left(G-SA_h^{-1}B\right)\mathbf{E}^q=-\mathbf{T}^q+SA_h^{-1}\mathbf{T}^u. \quad (5.3)$$

Note that solvability of the above linear system has been shown in [39]. We first prove that the right hand side above is bounded by Ch^2. Since the interpolation for the flux jump condition is a second order one, we have $\|\mathbf{T}^q\|_\infty \le Ch^2$. For the second term, from the interpolation scheme in (4.23), we consider one component and carry out the derivation

$$
\begin{aligned}
(SA_h^{-1}\mathbf{T}^u)_k &= \sum_{|\mathbf{x}_{ij}-\mathbf{X}_k|\le\delta_h} \gamma_{ij}\,(A_h^{-1}\mathbf{T}^u)_{ij}\\
&= \sum_{|\mathbf{x}_{ij}-\mathbf{X}_k|\le\delta_h} \gamma_{i,j}\sum_{l,r} G^h(\mathbf{x}_{lr},\mathbf{x}_{ij})\,h^2\,\tau_{lr}\\
&= \sum_{l,r} h^2\,\tau_{lr}\left(\sum_{|\mathbf{x}_{ij}-\mathbf{X}_k|\le\delta_h} \gamma_{i,j} G^h(\mathbf{x}_{lr},\mathbf{x}_{ij})\right),
\end{aligned}
\qquad (5.4)
$$

where $G^h(\mathbf{x}_{lr}, \mathbf{x}_{ij})$ is the discrete Green function defined as

$$
\mathbf{G}^h(\mathbf{x}_{ij},\mathbf{x}_{lm}) = \left(A_h^{-1}\mathbf{e}_{lm}\frac{1}{h^2}\right)_{ij}, \qquad \mathbf{G}^h(\partial\Omega_h,\mathbf{x}_{lm})=0, \qquad (5.5)
$$

where $\mathbf{e}_{lm}$ is the unit grid function whose values are zero at all grid points except at $\mathbf{x}_{lm} = (x_l, y_m)$ where its component is $e_{lm} = 1$, see for example [21]. Note that in the neighborhood of $|\mathbf{x}_{ij} - \mathbf{X}_k| \le \delta_h$, the points involved in the interpolation is close to $\mathbf{X}_k$, we can continue to derive

$$
\begin{aligned}
(SA_h^{-1}\mathbf{T}^u)_k &= \sum_{l,r} h^2\,\tau_{lr}\left(\sum_{|\mathbf{x}_{ij}-\mathbf{X}_k|\le\delta_h}\gamma_{i,j}\left(G_I^h(\mathbf{x}_{lr},\mathbf{X}_k) + h\frac{G^h(\mathbf{x}_{lr},\mathbf{x}_{ij})-G_I^h(\mathbf{x}_{lr},\mathbf{X}_k)}{h}\right)\right)\\
&= \sum_{l,r} h^2\,\tau_{lr}\left(\sum_{|\mathbf{x}_{ij}-\mathbf{X}_k|\le\delta_h}\gamma_{i,j} G_I^h(\mathbf{x}_{lr},\mathbf{X}_k)\right) + \sum_{l,r} h^3\,\tau_{lr}\left(\sum_{|\mathbf{x}_{ij}-\mathbf{X}_k|\le\delta_h}\gamma_{i,j}\left(\frac{\partial G_I^h(\mathbf{x}_{lr},\mathbf{X}_k)}{\partial\mathbf{x}}\right)+O(h)\right)\\
&= \sum_{l,r} h^3\,\tau_{lr}\left(\sum_{|\mathbf{x}_{ij}-\mathbf{X}_k|\le\delta_h}\gamma_{i,j}\left(\frac{\partial G_I^h(\mathbf{x}_{lr},\mathbf{X}_k)}{\partial\mathbf{x}}\right)+O(h)\right).
\end{aligned}
$$

The first term in the top line above is zero due to the consistency of the interpolation scheme for the flux jump condition. We have $|\tau_{lr}| \le Ch^2$ and at regular grid points, and $|\tau_{lr}| \le Ch$ at irregular grid points, from the estimate of $\frac{\partial G_I^h}{\partial \mathbf{x}}$ (3.16) in [41] we further derive

$$
\begin{aligned}
|(SA_h^{-1}\mathbf{T}^u)_k| &\le \sum_{l,r} h^3|\tau_{lr}|\left(\sum_{|\mathbf{x}_{ij}-\mathbf{X}_k|\le\delta_h}|\gamma_{ij}|\left(\frac{C}{(\|\mathbf{x}_{lr}-\mathbf{X}_k\|_2+h)}\right)+O(h)\right)\\
&\le \sum_{l,r,\Omega_h^{reg}} h^3|\tau_{lr}|\left(\sum_{|\mathbf{x}_{ij}-\mathbf{X}_k|\le\delta_h}|\gamma_{ij}|\left(\frac{C}{(\|\mathbf{x}_{lr}-\mathbf{X}_k\|_2+h)}\right)+O(h)\right) + \sum_{l,r,\Omega_h^{irr}} h^3|\tau_{lr}|\left(\sum_{|\mathbf{x}_{ij}-\mathbf{X}_k|\le\delta_h}|\gamma_{ij}|\left(\frac{C}{(\|\mathbf{x}_{lr}-\mathbf{X}_k\|_2+h)}\right)+O(h)\right)\\
&\le \sum_{l,r,\Omega_h^{reg}} h^4\left(\sum_{|\mathbf{x}_{ij}-\mathbf{X}_k|\le\delta_h}\left(\frac{C}{(\|\mathbf{x}_{lr}-\mathbf{X}_k\|_2+h)}\right)+O(h)\right) + \sum_{l,r,\Omega_h^{irr}} h^3\left(\sum_{|\mathbf{x}_{ij}-\mathbf{X}_k|\le\delta_h}\left(\frac{C}{(\|\mathbf{x}_{lr}-\mathbf{X}_k\|_2+h)}\right)+O(h)\right)\\
&\le h^2\sum_{|\mathbf{x}_{ij}-\mathbf{X}_k|\le\delta_h}\left(\sum_{l,r,\Omega_h^{reg}}\left(\frac{C}{(\|\mathbf{x}_{lr}-\mathbf{X}_k\|_2+h)}\right)h^2+O(h^3)\right) + h^2\sum_{|\mathbf{x}_{ij}-\mathbf{X}_k|\le\delta_h}\left(\sum_{l,r,\Omega_h^{irr}}\left(\frac{C}{(\|\mathbf{x}_{lr}-\mathbf{X}_k\|_2+h)}\right)h+O(h^3)\right)\\
&\le Ch^2|\log h| + Ch^2,
\end{aligned}
$$

where Ω_h^{irr} and Ω_h^{reg} are the sets of all irregular and regular grid points, respectively. In the derivation above we have used the facts that $|\gamma_{ij}| \sim 1/h$, $|\tau_{Ir}| \le Ch^2$ at regular grid points and $|\tau_{Ir}| \le Ch$ at irregular grid points, respectively. We have also used the estimate of the Riemann sum for the double integral $\int\int 1/(x^2+y^2+h)dxdy \le C|\log h|$. Note also that the total number of regular grid points is $O(1/h^2)$ while the total number of irregular grid points is $O(1/h)$. It has been shown that Schur complement matrix A_h^{schur} is non-singular, thus we have $\|A_h^{schur}\mathbf{E}^q\|_\infty \le Ch^2|\log h|$.

We have shown that the right hand side for the error of the augmented variable has the order of $h^2 \log h$. From Section 6.1.2 in [43], we know that the left hand side of (5.3) is

$$A_h^{schur}\mathbf{E}^q = \left[\beta\frac{\partial\tilde{\mathbf{U}}}{\partial n}(\mathbf{E}^q)\right] - \left[\beta\frac{\partial\tilde{\mathbf{U}}}{\partial n}(\mathbf{0})\right], \quad (5.6)$$

where $\tilde{\mathbf{U}}(\mathbf{E}^q)$ can be regarded as the solution of the numerical method applied to the following problem

$$\nabla\cdot(\beta\nabla\tilde{u}) = \mathbf{T}_I^u(\mathbf{x}); \quad \tilde{u}|_{\partial\Omega} = 0, \quad (5.7)$$

$$[\tilde{u}]_\Gamma = 0, \quad \left[\beta\frac{\partial\tilde{u}}{\partial n}\right]_\Gamma = \mathbf{T}_I^q(\mathbf{X}), \quad (5.8)$$

where $\mathbf{T}_I^u(\mathbf{x}) \in C$ is an interpolation function of $\mathbf{T}^u$ on the entire domain while $\mathbf{T}_I^q(\mathbf{X}) \in C$ is an interpolation function of $\mathbf{T}^q$ along the interface. From the maximum principal, we know that $|\tilde{u}| \le Ch^2$ and $\left|\frac{\partial\tilde{u}^\pm}{\partial n}\right| \le Ch^2$. Therefore the second term in (5.6) is bounded by Ch^2. Thus we have

$$\begin{aligned} A_h^{schur}\mathbf{E}^q = \left[\beta\frac{\partial\tilde{\mathbf{U}}}{\partial n}(\mathbf{E}^q)\right] &= \beta^+\frac{\partial\tilde{\mathbf{U}}}{\partial n}^+(\mathbf{E}^q) - \beta^-\frac{\partial\tilde{\mathbf{U}}}{\partial n}^-(\mathbf{E}^q) + O(h^2) \\ &= \beta^+\mathbf{E}^q - [\beta]\frac{\partial\tilde{\mathbf{U}}}{\partial n}^-(\mathbf{E}^q) + O(h^2), \end{aligned}$$

since β is a piecewise constant that has been divided by, from [8], we know that the solution and the derivative are both second order accurate when the IIM is applied, which implies that $\|\frac{\partial\tilde{\mathbf{U}}}{\partial n}^-(\mathbf{E}^q)\|_\infty \le Ch^2$. We have already proved that $\|A_h^{schur}\mathbf{E}^q\|_\infty \le Ch^2$, this leads to $\|\mathbf{E}^q\|_\infty \le Ch^2$.

<u>**Remark 5.3:**</u> *In the preconditioning strategy, we can write, for example, equation (6.24) in* [43],

$$\frac{\partial \tilde{\mathbf{U}}}{\partial n}^{-}(\mathbf{E}^q)=\gamma\left[\beta\frac{\partial \tilde{\mathbf{U}}}{\partial n}(\mathbf{E}^q)\right]+F_\Gamma+O(h^2), \qquad (5.9)$$

where γ is a constant, and F_Γ is a vector, then we have

$$\begin{aligned}A_h^{schur}\mathbf{Q}=&\left[\beta\frac{\partial \mathbf{U}}{\partial n}(\mathbf{Q})\right]-\left[\beta\frac{\partial \mathbf{U}}{\partial n}(\mathbf{0})\right]=\beta^+\frac{\partial \mathbf{U}}{\partial n}^{+}(\mathbf{Q})-\beta^-\frac{\partial \mathbf{U}}{\partial n}^{-}(\mathbf{Q})-\left[\beta\frac{\partial \mathbf{U}}{\partial n}(\mathbf{0})\right]\\ =&(\beta^+-\beta^-\gamma)\,\mathbf{Q}-\beta^-F_\Gamma-\left[\beta\frac{\partial \mathbf{U}}{\partial n}(\mathbf{0})\right]+O(h^2),\end{aligned}$$

which means that the Schur complement matrix is nearly a diagonal. This may explain why the number of the GMRES iterations is independent of the mesh size and the jump in β. For variable coefficient $\beta(\mathbf{x})$, with the new preconditioning strategy, we would have

$$A_h^{schur}\mathbf{Q}==D(\overline{\beta}(\mathbf{x}))\mathbf{Q}+\tilde{\mathbf{F}}_\Gamma+O(h^2),$$

where $D(\bar{\beta}(\mathbf{x}))$ is a diagonal matrix whose entries are $(\beta_k^+-\beta_k^-)/\overline{\beta}_k$, $\overline{\beta}_k=(\beta_k^++\beta_k^-)/2$.

Remark 5.4: *While the proof above is for piecewise constant coefficient, the conclusion is also true, or at least asymptotically in terms of h, for variable coefficient $\beta(\mathbf{x}) \geq \beta_0 > 0$ assuming that $\beta(\mathbf{x}) \in C^\infty(\Omega^\pm)$ since those terms involved are lower order terms of h. This is because the coefficient matrix $A_h(\beta) = A_h(I + B_h)$ and $\|B_h\| \to 0$ as $h \to 0$, where A_h is the discrete Laplacian. This is another advantage using the reformulated PDE.*

6. Numerical examples

We present a variety of numerical experiments to show the performance of the new augmented method for accurate solutions and its first order gradient at the interface. All the experiments are computed with the double precision and are performed on a desktop computer with Pentium(R) Dual-Core CPU, 2.59 GHz, 4GB memory. We also list the CPU time (s) in tables. We present errors in L^∞ norms and estimate the convergence order using

$$r=\frac{1}{\log 2}\log\frac{\|\mathbf{E}_{2h}\|_\infty}{\|\mathbf{E}_h\|_\infty}.$$

The tolerance of the GMRES iteration is set to be 10^{-6} and the initial value is set to be **0** in all computations. In all tables listed in this section, we use "Iter" to represent the number of GMRES iterations, "N_b" the number of control points, "N" the number of the grid lines in each direction of the rectangular domain and "CPU(s)" the run time in seconds.

Example 6.1:

$$u(\mathbf{x})=\begin{cases}\sin(x+y) & in\,\Omega^-,\\ \log(x^2+y^2) & in\,\Omega^+,\end{cases}\qquad \beta(\mathbf{x})=\begin{cases}\sin(x+y)+2 & in\,\Omega^-,\\ \cos(x+y)+2 & in\,\Omega^+,\end{cases} \quad (6.1)$$

where the interface is the zero level set of $\varphi(x,y)=\sqrt{x^2+y^2}-0.5$*, and* Ω = [−1, 1]× [−1, 1]. *The source term* $f(\mathbf{x})$*, and the interface jump conditions: [u] and [*βu_n*] are derived from the exact solution.*

This is an almost arbitrary example with a genuine piecewise smooth non-linear solution, and a variable coefficient with a variable discontinuity along the interface. We present a grid refinement analysis in Table 2. The second column is the maximum error of the solution while the third column is the approximate convergence order. The fourth and sixth column are the errors of the normal derivatives at the interface from Ω^- and Ω^+ sides, respectively. The fifth and seventh columns are the approximate convergence order of the computed normal derivative. The last but two column is the number of is the number of GMRES iterations, and the last but one is orthogonal projections of irregular grid points from Ω^+ side. The last column is the total CPU time in second. We can observe from Table 2 that the new augmented IIM is second order accurate both in the solution globally and the gradient at the interface from each side. The total CPU time also shows that the method is very fast with the optimal computational complexity ($O(N^2)\log(N^2)$). We also observe that the number of GMRES iteration is a constant independent of the mesh size.

Now we use the same exact solution and interface but with a large jump in the coefficient along the interface

$$\beta(\mathbf{x})=\begin{cases}10e^{10x} & \text{in}\,\Omega^-,\\ \sin(x+y)+2 & \text{in}\,\Omega^+.\end{cases} \quad (6.2)$$

The jump ratio varies from 1 : 10 to 1.45 : 1482 along the interface, a quite dramatic change. The results are shown in Table 3. We observe that the errors are larger than that in Table 2. This is due to the variations of the coefficient. Since the re-scaled PDE has the form $\Delta u+\frac{1}{\beta}\nabla\beta(x)\cdot\nabla u+\cdots$, we would expect the error term contains $\frac{\beta_x}{\beta}u_x$ and $\frac{\beta_y}{\beta}u_y$ that are $O(1)$ for Table 2 and $O(10^2)$ for Table 3 due to the term $10e^{10x}$. This explains well in the difference in the errors. Nevertheless, all the nice features are the same as the previous example.

An example with more general jump conditions

There are some applications in which we may have more general jump conditions. Here we consider an example with a more general jump condition, $c(\mathbf{X})u_n^+-d(\mathbf{X})u_n^-=v(\mathbf{X})$ with $c(\mathbf{X}) = x^2+1$, $d(\mathbf{X}) = y^2 + 1$. Our method still can work with the modified augmented equation (4.25) (now it is $c(\mathbf{X})u_n^+-d(\mathbf{X})u_n^-=v(\mathbf{X})$) and different preconditioning techniques. The convergency analysis may not apply directly anymore. In Table 4, we list the grid refinement analysis which has the same predicted convergency and efficiency.

Example 6.2: A general interface example with piecewise constant coefficient.

The example is from [39]. The interface is the zero level set function

$$\varphi(\mathbf{x})=r-(0.5+0.2\sin(5\theta)), \quad (6.3)$$

and the true solution is

$$u(\mathbf{x})=\begin{cases} \frac{r^2}{\beta^-} & \mathbf{x}\in\Omega^-, \\ \frac{r^4+C_0\log(2r)}{\beta^+} & \mathbf{x}\in\Omega^+. \end{cases} \quad (6.4)$$

The interface is both convex and concave and has relatively large curvature at some places, see Figure 1. We repeat this example with the new preconditioning technique with $\beta^+ = 1000$ and $\beta^- = 1$ on the domain $\Omega = [-1, 1] \times [-1, 1]$. The results are shown in Table 5 that are almost the same as the original fast IIM in [39]. Once again we observe that both the solution and the gradient are second order accurate and the number of GMRES iterations is independent of the mesh size. For this example, the interface has large curvature at some places. We need a reasonable fine mesh to resolve the interface.

6.1. An example for more general self-adjoint elliptic interface problems

With some modifications, the method developed in this paper has been generalized to more general interface problems

$$\nabla\cdot(\beta(\mathbf{x})\nabla u(\mathbf{x}))-\sigma(\mathbf{x})u(\mathbf{x})=f(\mathbf{x}). \quad (6.5)$$

The regularity requirement for the existence of the solution includes additional conditions $\sigma(\mathbf{x}) \in C(\Omega^\pm)$ and $\sigma(\mathbf{x}) \geq 0$. While we still get second order accuracy both in the solution and the gradient, the coefficient matrix from the modified algorithm may not be an M-matrix anymore. Nevertheless, those affected entries are of $O(1)$ compared $O(1/h^2)$ when $\sigma(\mathbf{x}) = 0$, that is, $A_h^{\sigma\neq 0}=A_h^{\sigma=0}(I+B_h)$ with $\|B_h\| \leq Ch^2$. Thus we have asymptotic convergence as those presented in the paper as $h \to 0$.

Example 6.3: *A general example with $\sigma(\mathbf{x}) \neq 0$. We present a more general example with a non-zero $\sigma(\mathbf{x})$ term with different interfaces, an ellipse and a five-star. The true solution and coefficient are*

$$u(\mathbf{x})=\begin{cases} -x^3+2y^3 & in\,\Omega^-, \\ \sin(x+y) & in\,\Omega^+, \end{cases} \qquad \beta(\mathbf{x})=\begin{cases} 1+e^{x+2y} & in\,\Omega^-, \\ \sin(2x-y)+3 & in\,\Omega^+, \end{cases} \quad (6.6)$$

$$\sigma(\mathbf{x})=\begin{cases} \cos(xy)+2 & in\,\Omega^-, \\ x^2+y^2+1 & in\,\Omega^+, \end{cases}, \quad (6.7)$$

where again $\Omega = [-1, 1]\times[-1, 1]$*. This is a very general example for a self-adjoint elliptic interface problem with non-linear solution. We test our method for two different interfaces.*

In Table 6, we show a grid refinement analysis for an elliptic interface $\varphi(x, y) = (x/0.6)^2+(y/0.4)^2-1$. We observe once again second order convergence for the global solution and the gradient at the interface.

In Table 7, we show a grid refinement analysis for a skinny ellipse $\varphi(x, y) = x^2 + (y/0.25)^2 - 1$ in the domain $[-1.5, 1.5] \times [-1.5, 1.5]$. Once we have the mesh fine enough to resolve the interface (here $N \geq 64$), we observe once again second order convergence for the global solution and the gradient at the interface although the largest error often appears near the tips of the longer axis of the ellipse.

If we increase the aspect ratio of the ellipse further, we can approximate the situations in which the domain has cracks, see Figure 5 in which we tried to find the electric potential in a domain containing an approximated crack $\varphi(x, y) = (x/0.5)^2 + (y/0.0625)^2 - 1$ within the domain $[-1, 1] \times [-1, 1]$. In this case, we have the PDE $\nabla \cdot (\beta\nabla u) = 0$, $[u]_\Gamma = 0$ and $[\beta u_n] = 0$, where β is the conductivity. The potential is given at the boundary with high potential on the right. Figure 5 (a) is the case with the ratio $\beta^+ : \beta^- = 1 : 1000$, while Figure 5 (b) the ratio is $\beta^+ : \beta^- = 1000 : 1$. Note that, we have tested the code against the analytic solution (6.6) for which we get the same convergence order. More sophisticated techniques and analysis can be found in [17, 64, 56, 52, 63].

In Table 8, we show a grid refinement analysis for the five-star interface $\varphi(x, y) = r - (0.5 + 0.2 \sin \theta)$ in polar coordinates (r, θ), $0 \leq \theta < 2\pi$. While we still observe average second order convergence for the global solution and the gradient at the interface, the errors are fluctuated more even though the average convergence rate is the same, compared with the elliptic interface. We do observe that again for complicated interfaces, we need to resolve the interface for an accurate solution and its gradient.

7. Conclusions

In this paper, we proposed a new augmented immersed interface method for general elliptic interface problems with variable coefficients that have finite jumps across a general interface, and non-homogeneous jump conditions. Not only the computed solution is second order globally, but also its gradient at the interface from each side of the interface. The method is designed for closed smooth interfaces not for open-ended interface such as cracks.

For closed interfaces but with corners, the method still can work with possible large errors near the corners. The convergence of method has been shown both in one and two dimensions under appropriate regularity assumptions and a piecewise constant $\beta(\mathbf{x})$. For a variable coefficient $\beta(\mathbf{x})$, the conclusions are still true if h is small enough, that is, in the asymptotic sense. Whether this can be improved and why the preconditioning technique works well are two open questions.

Acknowledgments

The authors would like to thank Dr. Thomas Beale of Duke University for valuable discussions. We thank the help from Dr. Guanyu Chen, a formal graduate student at NCSU. We would like also to thank anonymous referees for useful suggestions which helped us to improve the quality of the paper. The first and third authors are partially supported by an NSF grant DMS-1522768, NIH grant 5R01GM96195-2, and CNSF grants 11371199 and 11471166, and BK201411443. The second author is partially supported by a grant BK20160880 from the Natural Science Foundation of Jiangsu Province, China.

References

1. Albright J, Epshteyn Y, Steffen KR. High-order accurate difference potentials methods for parabolic problems. Appl Numer Math. 2015; 93:87–106.
2. Albright, Jason, Epshteyn, Y., Medvinsky, M., Xia, Q. High-order numerical schemes based on difference potentials for 2D elliptic problems with material interfaces. 2016 submitted.
3. Auchmuty G, Klouček P. Spectral solutions of self-adjoint elliptic problems with immersed interfaces. Appl Math Optim. 2011; 64(3):313–338.
4. Auchmuty, Giles. Steklov eigenproblems and the representation of solutions of elliptic boundary value problems. Numer Funct Anal Optim. 2004; 25(3–4):321–348.
5. Auchmuty, Giles. Spectral characterization of the trace spaces $H^s(\partial\Omega)$. SIAM J Math Anal. 2006; 38(3):894–905. (electronic).
6. Auchmuty, Giles, Klouček, Petr. Generalized harmonic functions and the dewetting of thin films. Appl Math Optim. 2007; 55(2):145–161.
7. Babuška I. The finite element method for elliptic equations with discontinuous coefficients. Computing. 1970; 5:207–213.
8. Beale JT, Layton AT. On the accuracy of finite difference methods for elliptic problems with interfaces. Commun Appl Math Comput Sci. 2006; 1:91–119.
9. Bramble J, King J. A finite element method for interface problems in domains with smooth boundaries and interfaces. Advances in Comput Math. 1996; 6:109–138.
10. Camp B, Lin T, Lin Y, Sun W. Quadratic immersed finite element spaces and their approximation capabilities. Adv Comput Math. 2006; 24:81–112.
11. Cannon, John R., Primicerio, Mario. A two phase Stefan problem with flux boundary conditions. Ann Mat Pura Appl. 1971; 88(4):193–205.
12. Chen S, Merriman B, Smereka P, Osher S. A fast level set based algorithm for Stefan problems. J Comput Phys. 1997; 135:8–29.
13. Chen Z, Zou J. Finite element methods and their convergence for elliptic and parabolic interface problems. Numer Math. 1998; 79:175–202.
14. Chou S, Kwak D, Wee K. Optimal convergence analysis of an immersed interface finite element method. Advances in Computational Mathematics. 2010; 33:149–168.
15. Epshteyn Y, Medvinsky M. On the Solution of the Elliptic Interface Problems by Difference Potentials Method. Springer Volume of Lecture Notes in Computational Science and Engineering (LNCSE) Series. 2015; 106:197–205.
16. Epshteyn Y, Phippen S. High-order difference potentials methods for 1d elliptic type models. Appl Numer Math. 2015; 93:69–86.
17. Feng X, Li Z, Wang L. Analysis and numerical methods for some crack problems. Int J Num Anal & Model, Series B. 2011; 2:155–166.

18. Furzeland RM. A comparative study of numerical methods for moving boundary problems. J Inst Maths Applics. 1980; 26:411–429.
19. Gilbarg, David, Trudinger, Neil S. Classics in Mathematics. Springer-Verlag; Berlin: 2001. Elliptic partial differential equations of second order. Reprint of the 1998 edition
20. Gong Y, Li B, Li Z. Immersed-interface finite-element methods for elliptic interface problemswith non-homogeneous jump conditions. SIAM J Numer Anal. 2008; 46:472–495.
21. Hackbusch, W. Elliptic Differential Equations: Theory and Numerical Treatment. Springer-Verlag; 1992.
22. Han H. The numerical solutions of the interface problems by infinite element methods. Numer Math. 1982; 39:39–50.
23. Hansbo A, Hansbo P. An unfitted finite element method, based on Nitsche's method, for elliptic interface problems. Comput Methods Appl Mech Engrg. 2002; 191:5537–5552.
24. He X, Lin T, Lin Y. Approximation capability of a bilinear immersed finite element space. Numerical Methods for Partial Differential Equations. 2008; 24:1265–1300.
25. He X, Lin T, Lin Y. Immersed finite element methods for elliptic interface problems with non-homogeneous jump conditions. Int J Numer Anal Model. 2010
26. He X, Lin T, Lin Y. The convergence of the bilinear and linear immersed finite element solutions to interface problems. Numerical Methods for Partial Differential Equations. 2012; 28:312–330.
27. Hellrung J, Wang L, Sifakis E, Teran J. A second-order virtual node method for elliptic problems with interfaces and irregular domains in three dimensions. J Comput Phys. 2012; 231:2015–2048.
28. Hou S, Li Z, Wang L, Wang W. A numerical method for solving elasticity equations with sharp-edged interfaces. Commun Comput Phys. 2012; 12:595–612. [PubMed: 22707984]
29. Hou S, Liu X. A numerical method for solving variable coefficient elliptic equation with interfaces. J Comput Phys. 2005; 202:411–445.
30. Hou T, Li Z, Osher S, Zhao H. A hybrid method for moving interface problems with application to the Hele-Shaw flow. J Comput Phys. 1997; 134:236–252.
31. Hou T, Wu X, Zhang Y. Removing the cell resonance error in the multiscale finite element method via a Petrov-Galerkin formulation. Comm Math Sci. 2004; 2:185–205.
32. Hou TY, Lowengrub JS, Shelley MJ. Removing the stiffness from interfacial flows with surface tension. J Comput Phys. 1994; 114:312–338.
33. Kevorkian, J. Partial Differential Equations. Wadsworth & Brooks/Cole; 1990.
34. Klouček, Petr, Sorensen, Danny C., Wightman, Jennifer L. The approximation and computation of a basis of the trace space $H^{1/2}$. J Sci Comput. 2007; 32(1):73–108.
35. Kwak D, Wee K, Chang K. An analysis of a broken P_1-nonconforming finite element method for interface problems. SIAM J Numer Anal. 2010; 48:2117–2134.
36. Layton, William J., Schieweck, Friedhelm, Yotov, Ivan. Coupling fluid flow with porous media flow. SIAM J Numer Anal. 2003; 40:2003.
37. LeVeque, RJ. Finite Difference Methods for Ordinary and Partial Differential Equations, Steady State and Time Dependent Problems. SIAM; 2007.
38. LeVeque RJ, Li Z. The immersed interface method for elliptic equations with discontinuous coefficients and singular sources. SIAM J Numer Anal. 1994; 31:1019–1044.
39. Li Z. A fast iterative algorithm for elliptic interface problems. SIAM J Numer Anal. 1998; 35:230–254.
40. Li Z. The immersed interface method using a finite element formulation. Applied Numer Math. 1998; 27:253–267.
41. Li Z. On convergence of the immersed boundary method for elliptic interface problems. Math Comp. 2015; 84(293):1169–1188.
42. Li Z, Ito K. Maximum principle preserving schemes for interface problems with discontinuous coefficients. SIAM J Sci Comput. 2001; 23:1225–1242.
43. Li, Z., Ito, K. The Immersed Interface Method – Numerical Solutions of PDEs Involving Interfaces and Irregular Domains. 2006. SIAM Frontier Series in Applied mathematics, FR33
44. Li Z, Lin T, Wu X. New Cartesian grid methods for interface problem using finite element formulation. Numer Math. 2003; 96:61–98.

45. Li Z, Soni B. Fast and accurate numerical approaches for Stefan problems and crystal growth. Numerical Heat Transfer, B: Fundamentals. 1999; 35:461–484.

46. Li Z, Xi L, Cai Q, Zhao H, Luo R. A semi-implicit augmented IIM for Navier-Stokes equations with open and traction boundary conditions. J Comput Phys. 2015; 297:182–193. [PubMed: 27087702]

47. Lin T, Lin Y, Sun W. Error estimation of a class of quadratic immersed finite element methods for elliptic interface problems. Discrete Contin Dyn Syst Ser B. 2007; 7

48. Lin T, Zhang X. Linear and bilinear immersed finite elements for planar elasticity interface problems. J Comput Appl Math. 2012; 236:4681–4699.

49. Lin, Tao, Lin, Yanping, Zhang, Xu. Partially penalized immersed finite element methods for elliptic interface problems. SIAM J Numer Anal. 2015; 53(2):1121–1144.

50. Liu J. Open and traction boundary conditions for the incompressible Navier-Stokes equations. J Comput Phys. 2009; 228:7250–7267.

51. Liu X, Fedkiw R, Kang M. A boundary condition capturing method for Poisson's equation on irregular domain. J Comput Phys. 2000; 160:151–178.

52. Martin, Vincent, Jaffré, Jérôme, Roberts, Jean E. Modeling fractures and barriers as interfaces for flow in porous media. SIAM J Sci Comput. 2005; 26(5):1667–1691. (electronic).

53. Massjung R. An unfitted discontinuous Galerkin method applied to elliptic interface problems. SIAM J Numer Anal. 2012; 50:3134–3162.

54. Medvinsky M, Tsynkov S, Turkel E. The method of difference potentials for the Helmholtz equation using compact high order schemes. J Sci Comput. 2012; 53(1):150–193.

55. Mitchell SL, Vynnycky M. Finite-difference methods with increased accuracy and correct initialization for one-dimensional Stefan problems. Appl Math Comput. 2009; 215(4):1609– 1621.

56. Morales, Fernando, Showalter, RE. The narrow fracture approximation by channeled flow. J Math Anal Appl. 2010; 365(1):320–331.

57. Pruitt, Michael. Large time step maximum norm regularity of L-stable difference methods for parabolic equations. Numer Math. 2014; 128(3):551–587.

58. Pruitt, Michael. Maximum norm regularity of periodic elliptic difference operators. ESAIM. 2015

59. Ryaben'kii, Viktor S. Method of difference potentials and its applications, volume 30 of Springer Series in Computational Mathematics. Springer-Verlag; Berlin: 2002. Translated from the 2001 Russian original by Nikolai K. Kulman

60. Sukumar N, Chopp DL, Moran B. Extended finite element for three-dimensional fatigue crack propagation. Engineering Fracture Mechanics. 2003; 70:29–48.

61. Wahlbin, Lars B. Superconvergence in Galerkin finite element methods, volume 1605 of Lecture Notes in Mathematics. Springer-Verlag; Berlin: 1995.

62. Wang J, Xiu Y. A weak Galerkin finite element method for second-order elliptic problems. J Comput Appl Math. 2013; 241:103–115.

63. Wiegmann A. Analytic solutions of a multi-interface transmission problem and crack approximation. Inverse Problems. 2000; 16:401–411.

64. Wiegmann A, Li Z, LeVeque R. Crack jump conditions for elliptic problems. Applied Math Letters. 1999; 12:81–88.

65. Wu H, Xia Y. An unfitted *hp*-interface penalty finite element method for elliptic interface problems. 2010 arXiv:1007.2893.

66. Xu J. Error estimates of the finite element method for the 2nd order elliptic equations with discontinuous coefficients. J Xiangtan University. 1982; 1:1–5.

67. Yang X, Li B, Li Z. The immersed interface method for elasticity problems with interface. Dynamics of Continuous, Discrete and Impulsive Systems. 2003; 10:783–808.

68. Ying WJ, Henriquez CS. A kernel-free boundary integral method for elliptic boundary value problems. J Comput Phy. 2007; 227(2):1046–1074.

69. Zhang, Zhimin, Naga, Ahmed. A new finite element gradient recovery method: superconvergence property. SIAM J Sci Comput. 2005; 26(4):1192–1213. (electronic).

70. Zhou YC, Zhao S, Feig M, Wei GW. High order matched interface and boundary method for elliptic equations with discontinuous coefficients and singular sources. J Comput Phys. 2006; 213:1–30.

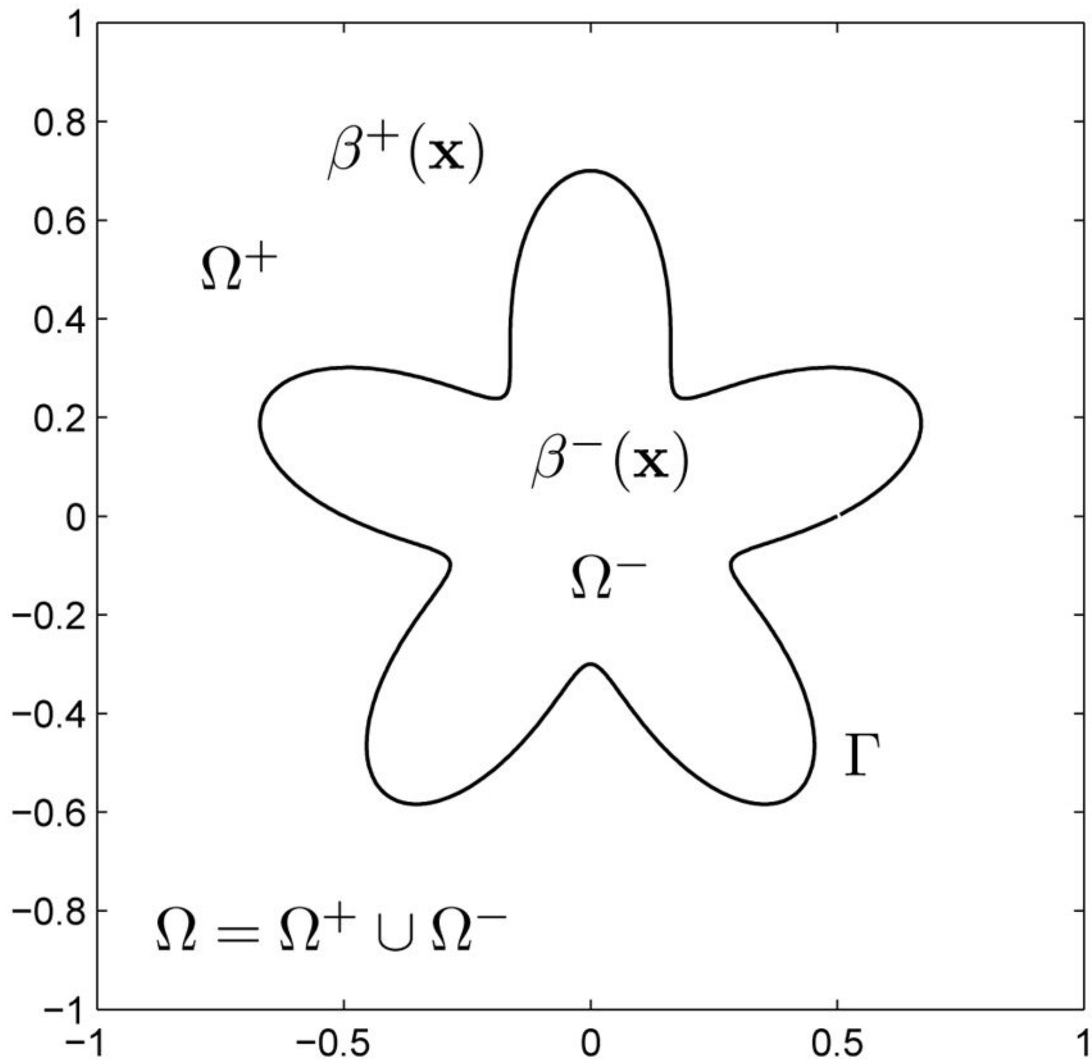

Fig. 1.

A diagram of a rectangular domain $\Omega = \Omega^+ \cup \Omega^-$ with an interface Γ. The coefficient $\beta(\mathbf{x})$ has a finite jump across the interface Γ. The interface and domain in this figure are used in Example 6.2 and Example 6.3 in Section 6.

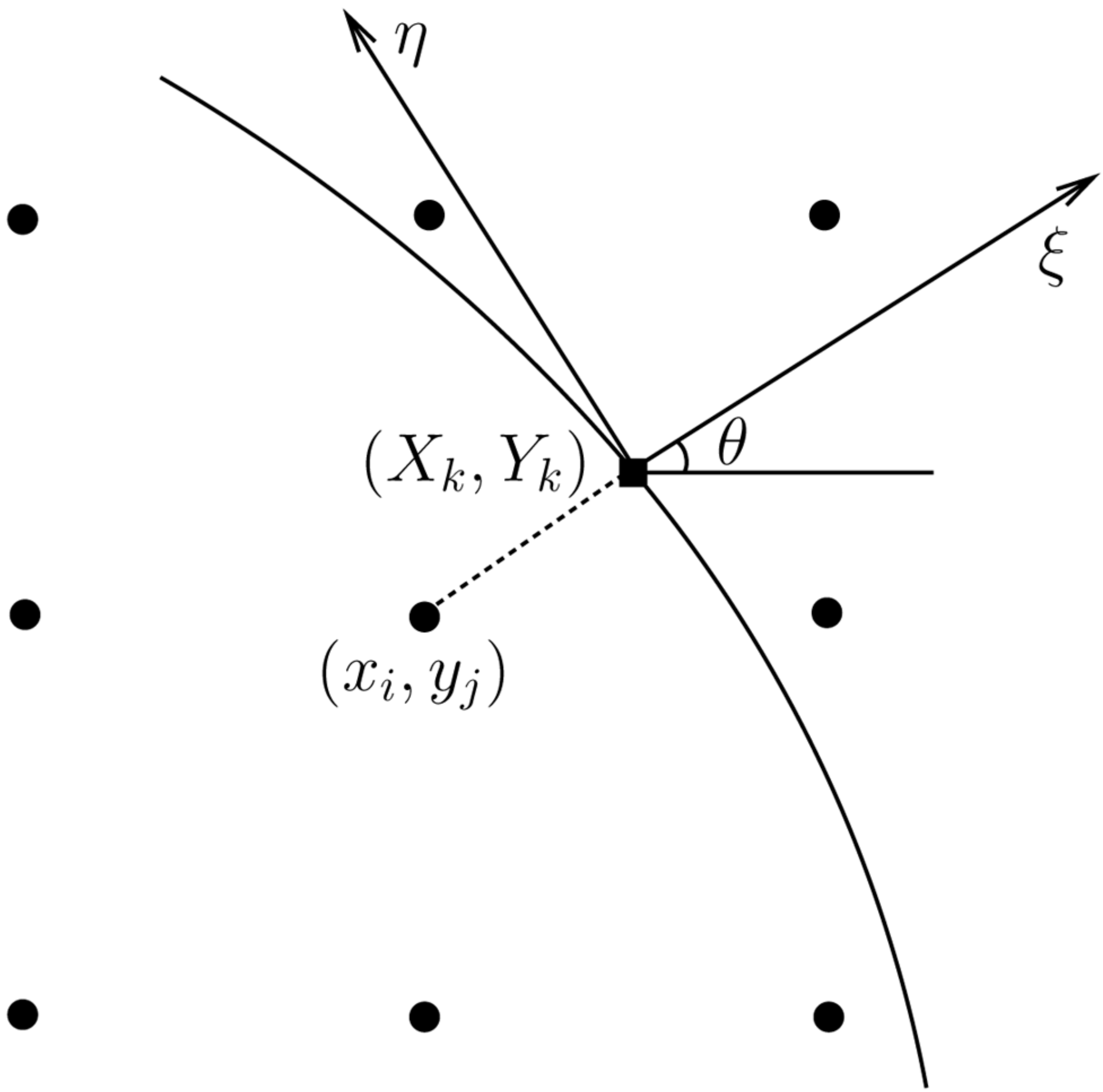

Fig. 2.
A diagram of an irregular grid point (x_i, y_j), its orthogonal projections on the interface (X_k, Y_k), and the local coordinates at (X_k, Y_k) in the normal and tangential directions.

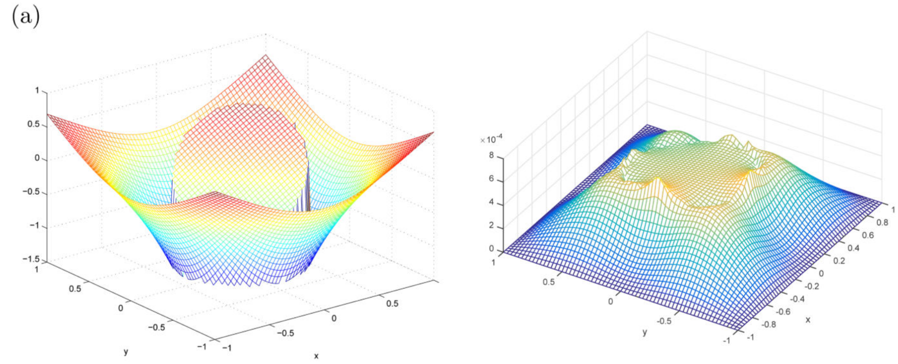

Fig. 3.

(a): The solution plot of Example 6.1. (b): The error plot of the computed solution. The error seems to be piecewise smooth as well which is important for accurate gradient computation.

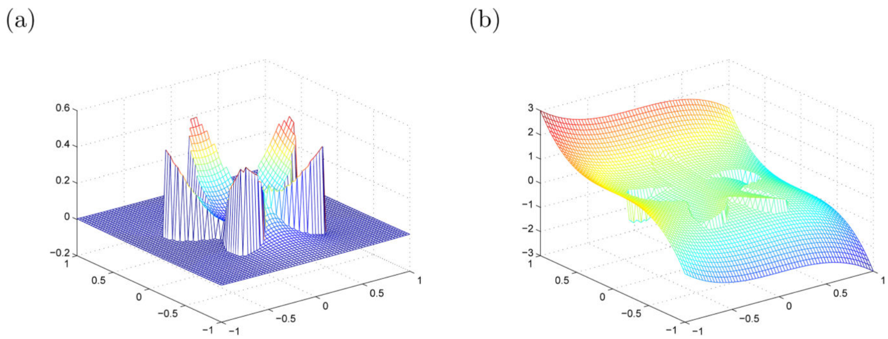

Fig. 4.
(a): The computed solution plot of Example 6.2. (b): The solution plot of Example 6.3.

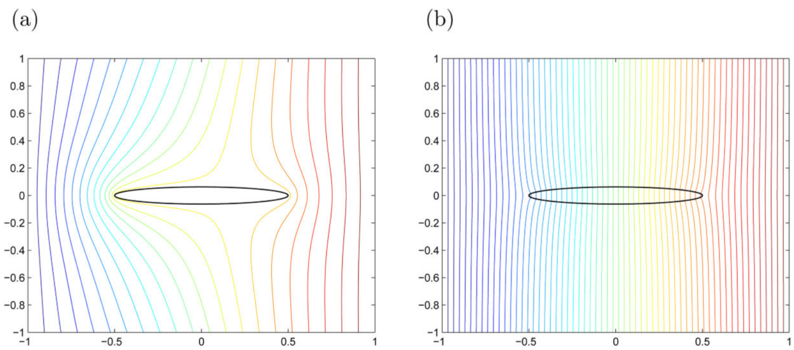

Fig. 5.

Electric potential in a domain containing a thin elliptic object. (a) The conductivity of the object is large (1 : 1000); (b) The conductivity of the object is small (1000 : 1).

Table 1

A grid refinement analysis for the Stefan problem at the final time $t = 3$. The computed solution, the first order derivative $u_x^-(\alpha(t))$, and the free boundary $\alpha(t)$ all have average second order convergence.

N	$\|\|u - U\|\|_\infty$	r	$\|[u_x] - Q\|$	r	$\|\alpha - \mathscr{A}\|$	r
16	2.3160×10^{-2}		3.9232×10^{-4}		4.0734×10^{-2}	
32	6.4260×10^{-3}	1.8496	3.0046×10^{-4}	0.3849	1.1473×10^{-2}	1.8280
64	1.9403×10^{-3}	1.7276	1.2357×10^{-5}	4.6038	3.5210×10^{-3}	1.7042
128	4.8957×10^{-4}	1.9867	1.8056×10^{-7}	6.0967	8.8986×10^{-4}	1.9843
256	1.0044×10^{-4}	2.2852	7.3479×10^{-8}	1.2971	1.7986×10^{-4}	2.3067

Table 2

A grid refinement analysis for Example 6.1 with a modest variable jump in the coefficient.

N	$E(u)$	r	$E(u_n^-)$	r	$E(u_n^+)$	r	Iter	N_b	CPU(s)
32	3.1245×10^{-3}		1.5905×10^{-2}		2.1712×10^{-2}		4	48	0.01
64	7.0327×10^{-4}	2.15	4.4752×10^{-3}	1.82	5.5256×10^{-3}	1.97	4	92	0.03
128	1.1565×10^{-4}	2.60	1.1182×10^{-3}	2.00	1.3993×10^{-3}	1.98	4	184	0.11
256	2.7720×10^{-5}	2.06	2.9096×10^{-4}	1.94	3.7998×10^{-4}	1.88	4	364	0.46
512	6.2087×10^{-6}	2.15	7.3489×10^{-5}	1.98	9.8004×10^{-5}	1.95	4	728	2.45

Table 3

A grid refinement analysis for Example 6.1 with a large variation in the jump ratio of the coefficient.

N	$E(u)$	r	$E(u_n^-)$	r	$E(u_n^+)$	r	Iter	N_b	CPU(s)
32	6.0115×10^{-1}		3.9014		1.7570		11	48	0.02
64	1.4706×10^{-1}	2.03	8.6974×10^{-1}	2.16	4.2479×10^{-1}	2.04	10	92	0.07
128	4.3411×10^{-2}	1.76	2.5265×10^{-1}	1.78	1.2537×10^{-1}	1.76	10	184	0.27
256	1.1266×10^{-2}	1.94	6.5293×10^{-2}	1.95	3.2493×10^{-2}	1.94	10	364	1.24
512	2.9178×10^{-3}	1.94	1.6916×10^{-2}	1.94	8.4205×10^{-3}	1.94	10	728	7.85

Table 4

A grid refinement analysis with a different jump condition $c(\mathbf{X})u_n^{+} - d(\mathbf{X})u_n^{-} = v(\mathbf{X})$.

N	*E(u)*	*r*	$E(u_n^-)$	*r*	$E(u_n^+)$	*r*	Iter	N_b	CPU(s)
32	1.0220×10^{-2}		2.4784×10^{-2}		2.5529×10^{-2}		4	48	0.047
64	2.9257×10^{-3}	1.80	6.5909×10^{-3}	1.91	6.2884×10^{-3}	2.02	4	92	0.172
128	7.9724×10^{-4}	1.87	1.7941×10^{-3}	1.87	1.5052×10^{-3}	2.06	4	184	0.578
256	2.0781×10^{-4}	1.93	4.6908×10^{-4}	1.93	3.7353×10^{-4}	2.01	4	364	2.531
512	5.3324×10^{-5}	1.96	1.2033×10^{-4}	1.96	9.5584×10^{-5}	1.96	4	728	10.141
1024	1.3253×10^{-5}	2.00	3.7729×10^{-5}	1.67	3.0206×10^{-5}	1.66	4	1452	44.281

Table 5

A grid refinement analysis for Example 6.2 with a piecewise constant coefficient $\beta^+ = 1000$ and $\beta^- = 1$ and a complicated interface.

N	$E(u)$	r	$E(u_n^-)$	r	$E(u_n^+)$	r	Iter	N_b	CPU(s)
32	1.2880×10^{-1}		3.0969		3.0971×10^{-3}		14	78	0.04
64	1.9431×10^{-1}	−0.59	4.0397	−0.38	4.0396×10^{-3}	−0.38	14	154	0.13
128	1.8734×10^{-2}	3.37	4.9723×10^{-1}	3.02	4.9765×10^{-4}	3.02	11	308	0.28
256	2.3009×10^{-3}	3.02	1.2096×10^{-1}	2.03	1.2352×10^{-4}	2.01	10	612	0.99
512	3.6351×10^{-4}	2.66	2.2790×10^{-2}	2.40	2.4786×10^{-5}	2.31	9	1226	21.50

Table 6

A grid refinement analysis for Example 6.3 for a general elliptic interface problems with the interface $(x/0.6)^2 + (y/0.4)^2 = 1$.

N	$E(u)$	r	$E(u_n^-)$	r	$E(u_n^+)$	r	Iter	N_b	CPU(s)
32	8.4180×10^{-3}		9.0987×10^{-2}		8.0826×10^{-2}		4	48	0.10
64	9.0036×10^{-4}	3.22	2.3473×10^{-2}	1.95	1.9611×10^{-2}	2.04	4	96	0.20
128	1.5842×10^{-4}	2.50	4.1771×10^{-3}	2.49	3.6921×10^{-3}	2.40	4	188	1.60
256	3.7209×10^{-5}	2.09	1.0639×10^{-3}	1.97	9.4238×10^{-4}	1.97	4	372	3.02
512	9.3380×10^{-6}	1.99	3.2952×10^{-4}	1.69	2.4187×10^{-4}	1.96	4	740	15.02

Table 7

A grid refinement analysis for Example 6.3 for a general elliptic interface problems with the interface $x^2 + (y/0.25)^2 = 1$.

N	$E(u)$	r	$E(u_n^-)$	r	$E(u_n^+)$	r	Iter	N_b	CPU(s)
32	8.2459×10^{-2}		1.3352		1.2700		5	44	0.078
64	4.7769×10^{-2}	0.78	8.9448×10^{-1}	0.57	6.7590×10^{-1}	0.90	5	88	0.156
128	6.5830×10^{-3}	2.85	1.6557×10^{-1}	2.43	1.5748×10^{-1}	2.10	5	176	1.250
256	9.2772×10^{-4}	2.82	7.1232×10^{-2}	1.21	4.7413×10^{-2}	1.73	5	352	2.250
512	1.7125×10^{-4}	2.43	1.4364×10^{-2}	2.31	1.1780×10^{-2}	2.00	5	704	19.703
1024	4.5859×10^{-5}	1.90	3.3351×10^{-3}	2.10	2.7234×10^{-3}	2.11	5	1408	77.812

Table 8

A grid refinement analysis for Example 6.3 for a general elliptic interface problems with a five-star interface, see Figure 1.

N	$E(u)$	r	$E(u_n^-)$	r	$E(u_n^+)$	r	Iter	N_b	CPU(s)
32	9.7746×10^{-1}		2.8683×10^{1}		4.7767		11	78	0.03
64	6.5486×10^{-2}	3.89	1.9417	3.88	3.2336×10^{-1}	3.88	10	154	0.10
128	1.5688×10^{-2}	2.06	6.4504×10^{-1}	1.58	1.0623×10^{-1}	1.60	9	308	0.29
256	1.8890×10^{-3}	3.05	1.6617×10^{-1}	1.95	3.6157×10^{-2}	1.55	9	612	1.07
512	3.8770×10^{-4}	2.28	2.9833×10^{-2}	2.47	6.7852×10^{-3}	2.41	9	1226	19.22